Worms or storms? Distinguishing bioturbation from physical mixing using multiple tracers

Tjitske J. Kooistra[1,3], Anna-Maartje de Boer[2], Tjeerd J. Bouma[1,3], Natascia Pannozzo[4], Stuart G. Pearson[4], Ad van der Spek[5], Henko de Stigter[6], Jakob Wallinga[2], Rob Witbaard[1], Karline Soetaert[1,3]

[1]Royal Netherlands Institute for Sea Research, Department of Estuarine and Delta Systems; Korringaweg 7, 4401 NT Yerseke.
[2]Wageningen University and Research, Soil Geography and Landscape group & Netherlands Centre for Luminescence dating; Droevendaalsesteeg 3, 6708 PB Wageningen.
[3]Faculty of Geoscience, Utrecht University, Princetonlaan 8a, 3584 CB Utrecht, the Netherlands.
[4]Faculty of Civil Engineering and Geosciences, Delft University of Technology, Stevinweg 1, 2628 CN Delft, The Netherlands.
[5]Deltares, Boussinesqweg 1, 2629 HV Delft, The Netherlands.
[6]Royal Netherlands Institute for Sea Research, Department of Ocean Systems, Landsdiep 4 1797 SZ 't Horntje.

Correspondence to: Tjitske J. Kooistra (tjitske.kooistra@nioz.nl)

Abstract. Sediment transport and seabed composition can both be influenced by bioturbation and hydrodynamically driven sediment mixing and deposition. In a dynamic intertidal environment, it is challenging to distinguish the relative contribution of both processes. We aim to unravel their relative importance by combining several tracers, each having its own specific timescale and target particle size. We combined (1) ^{210}Pb that quantifies long-term (years–decades) mixing of fine sediment fractions with (2) Chlorophyll-*a* and (3) luminophores that both quantify short-term mixing of fine sediment fractions (days–weeks), and (4) multi-grain quartz and single-grain feldspar luminescence dating, which use the bleaching of sand grains' inherent luminescence signal by light to assess mixing of sand and thereby quantifies long-term mixing. Single grain feldspar luminescence is here for the first time applied in the intertidal environment. We compare results for a sandy and a muddy intertidal flat at the island of Texel (Wadden Sea, the Netherlands), each with their own characteristic benthic community. Recent bioturbation became apparent from Chlorophyll-*a* and luminophore profiles: particles were rapidly reworked to a depth of decimetres. ^{210}Pb also suggested mixing and non-local exchange of particles by bioturbation. Luminescence age distributions suggest that quartz luminescence signals were fully reset upon recent deposition, while bioturbation enhanced resetting of feldspar luminescence signals. Coarse- and fine-grained tracer profiles show the differential behaviour and reworking of the mud and sand fraction within the sediment matrix: as expected with particle-selective bioturbation, mud is preferentially bioturbated and infiltrates passively, while sand grains have a higher ability to conserve layering. Single-grain feldspar luminescence is a promising technique to demonstrate the long-term reworking of sand grains, however, in young and dynamic environments, a combination of tracers remains necessary to inform on the origin of mixing.

Summary. On intertidal flats, it is hard to distinguish sediment mixing by animals from reworking by waves and currents. We used a combination of tracers to identify reworking of grains of different sizes on the short- and long term. Coarse (sand) grains were less mobile than fine (mud) grains, and partly kept their layering after deposition. The luminescence properties of sand grains can be used dating and can show sediment mixing, but this method needs to be tested more for young, intertidal sediments.
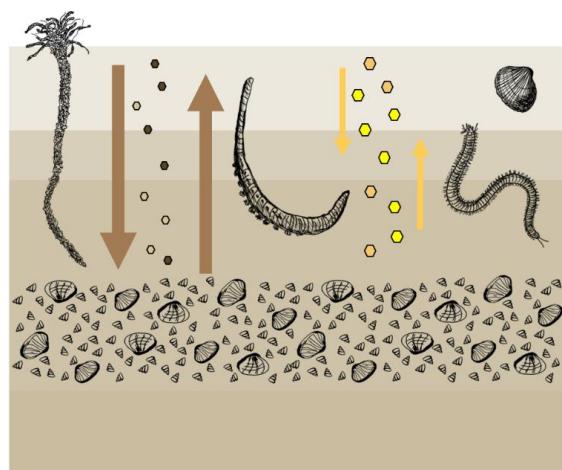
Summarising figure.

1. Introduction

In dynamic, soft-sediment seafloors, such as intertidal flats, sediment grain size is influenced by physical and ecological processes. The grain size composition of sediments determines sediment stability and erosion thresholds (Staudt et al., 2019). This, in turn, impacts daily sediment dynamics, and morphology on a larger spatial and temporal scale (Belliard et al., 2019). Sediment composition is also a crucial ecological factor, as it shapes the benthic community (e.g., Compton et al., 2013; Gray, 1974; Kooistra et al., 2025). It is therefore important to understand the drivers of grain-size distribution on intertidal flats. However, obtaining such knowledge is complicated, as the relevant interacting physical and ecological processes can act on different timescales.

Benthic animals e.g. like worms and bivalves can influence their sedimentary habitats by so-called 'bioturbation' (Davison 1891; Kristensen et al. 2012; Meysman et al. 2006; Richter 1952). With their burrowing, feeding and ventilating behaviour, they can influence the composition, stability, and density of the sediment (Jumars & Nowell 1984; Rhoads & Boyer 1982; Widdows & Brinsley 2002). This bioturbation has implications for biochemical cycling and carbon storage by remineralisation and burial of organic matter (Aller, 1982; Snelgrove et al., 2018). The mode of bioturbation differs per species: some randomly displace sediments over short distances (diffusive mixing), while others convey sediment upwards or downwards (advective transport) (François et al., 1997; Queirós et al., 2013). Moreover, bioturbators can be selective for particle size and type (Jumars et al. 1982; Taghon 1982).

Physical sediment deposition and reworking is dependent on periodic hydrodynamics, such as tidal currents, as well as waves and currents induced by meteorological conditions. During calm atmospheric conditions, spring- and neap tide periodicity can create layered bedding (Deloffre et al., 2007; Zhou et al., 2021), and tidal currents and wave forcing can result in a dynamic morphological equilibrium with bed level changes of 5–10 cm day^{-1} in macrotidal systems (Hu et al. 2015; Grandjean et al., 2023). In such systems, reworking by tidal current forcing is dominant at lower intertidal flats, while waves, generated by wind, are a major driver in the high intertidal (Belliard et al., 2019). High-energy events, such as storms, can transport large amounts of sediment over a short time span (de Vet et al., 2018). A storm can result in sediment relocations equivalent to at least months–years of sediment displacements under calm conditions, reworking sediment down to 15 cm depth (de Vet et al. 2020; Fan et al. 2006; Hu et al. 2018). Such intense meteorological events can deposit a coarse sand layer on a tidal flat (Zhou et al., 2022), or increase mud deposition by increasing inundation time and suspended sediment concentration as well as creating accommodation space by erosion (Colosimo et al. 2023; Gao 2018; Grandjean et al. 2023). Storm events can therefore be recognised in layering of the sediment bedding, where the timing relative to the spring-neap tidal cycle and storm chronology determines the storm layer grain size composition (Wang & Cheng 2016; Zhou et al. 2022b). This stratification can however largely be smoothed out by daily bioturbation, thereby erasing the signals of episodic deposition (Wheatcroft, 1990).

It is challenging to disentangle the biological from the physical control on sediment composition, i.e. to determine the extent to which 'turbation' is actually 'bio'. While on short timescales (days–weeks) and in controlled experiments, grains reworked by bioturbation can be clearly isolated from those reworked by hydrodynamics, on longer timescales (years–centuries) and in dynamic natural environments, this is nearly impossible. To obtain insight in the reworking processes in intertidal environments, acting at different frequencies and energy levels, we need tracers that gather information on short- and long-term reworking of different sediment fractions (Fig. 1). A short-term tracer needs to be exposed to a sufficient number of mixing events relative to its timescale, therefore

the spatial and temporal scale of sampling should match mixing intensity (Meysman et al., 2010). Long-term tracers may instead provide a more integrated result than short-term tracers, reflecting both long-term sediment
85   dynamics, as well as recent reworking. Vertical profiles can then inform on the short- and long-term reworking and deposition history. A strongly stratified profile might point to episodic deposition events, while a homogeneous signal over depth might indicate intense mixing by biota or hydrodynamics. Bioturbation might also cause sub-surface supply of young material through advective vertical transport (Meysman et al. 2003; Richter et al. 1996). Thus, combining signals can shed light on the origin of mixing processes acting in dynamic
90   coastal sediments.
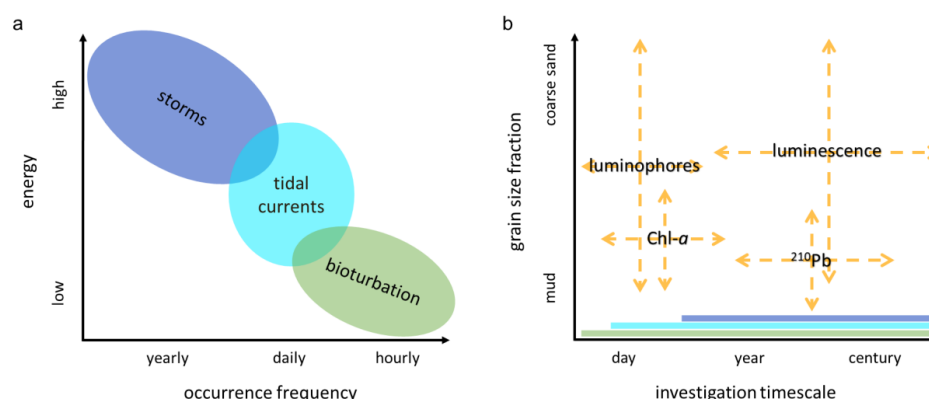
Figure 1: (a) mixing processes with their occurrence frequency and energy; (b) sediment tracers with their relevant investigation timescales and potential target sediment fraction. The mixing processes that are recorded in the tracer distributions, depending on the moment and period of sampling, are indicated as bands along the x-axis.

95   The relevant timescale and grain size fraction is specific for each tracer type (Table 1). Tracers that are commonly used for studying bioturbation in dynamic marine sediments have been previously reviewed by Maire et al. (2008). Here we highlight several commonly used tracers in the context of timescale and grain size. Tracers that give information on recent bioturbation are Chlorophyll-*a* (Chl-*a*) and luminophores. Due to its wide occurrence, Chl-*a* is often used as a tracer for bioturbation. Drawbacks are that the decay time varies with environmental conditions
100 (Sun et al., 1993), and herbivorous biota may actively select for Chl-*a* (Taghon, 1982). Luminophores are fluorescent coated particles that are commonly used to describe bioturbation over timescales of days to months to study particle size-specific and species- or community-specific mixing (Gerino et al., 1998; Montserrat et al., 2011). For longer-term sediment bioturbation, radioisotopes, with known half-lives, are commonly used in marine environments. One example is ^{210}Pb, which is produced in the atmosphere and water column in the naturally
105 occurring uranium decay chain and is deposited on the seafloor. After burial, ^{210}Pb activity decays until it reaches background levels. ^{210}Pb has been used to determine deposition and mixing of sediments, from the deep sea to estuarine and intertidal environments (Benninger et al., 1979; Richter et al., 1996).

Currently, tracers that allow to study mixing of sand-sized particles over long timescales in intertidal flats are lacking. One inherent characteristic of sand grains is their luminescence signal. This is a latent light signal that
110 builds up in minerals in response to exposure to ionizing radiation from the natural environment. The luminescence signals are reset upon exposure to light and thereby provide an estimate of the last light exposure of these minerals (i.e. the time grains were last at the surface).

Table 1. Tracers used in this study with their target grain size fraction, half-life time (Chl-*a* and ^{210}Pb) or bleaching time (luminescence signals). For the tracers with a half-life time, investigation timescales are 5x the tracer half-life (Lecroart et al. 2010; Meysman et al. 2008). Subaerial estimated bleaching times for luminescence signals are shown (Colarossi et al. 2015; Godfrey-Smith et al. 1988; Smedley et al. 2015).

Tracer	Sediment fraction	Half-life	Bleaching time (subaerial)	Investigation timescale
Luminophores	0–500 μm 0–125 μm (this study)	-		1–30 days
Chlorophyll-*a*	organic	3–250 days		15 days – 3 years
[210]Pb	< 63 μm, organic	22.3 years		111.5 years
Luminescence	6–250 μm (multi-grain) 212–250 μm (single-grain, this study)			10 years – 5 x 10⁶ years
Quartz OSL			seconds	up to 1.5 x 10⁵ years
Feldspar IRSL			seconds-minutes	up to 5 x 10⁵ years
Feldspar pIRIR			minutes-hours	up to 5 x 10⁵ years

Multi-grain quartz optically stimulated luminescence (OSL) has been applied for dating intertidal flat sediments (de Boer et al. 2024b; Madsen et al. 2005, 2007, 2011; Mauz & Bungenstock 2007; Mauz et al. 2010). In the terrestrial environment, luminescence methods are increasingly used to shed light on sediment mixing processes (Heimsath et al. 2002; Kristensen et al. 2015; Reimann et al. 2017; Stockmann et al. 2013; van der Meij et al. 2025; Zhang et al. 2025). Madsen et al. (2011) estimated sedimentation and bioturbation rates on an intertidal sandflat using large-aliquot quartz OSL on the grainsize 90 - 250 μm. However, this tracer only gives the average age of all luminescing grains in a subsample (often referred to as aliquot), which may be biased by a few older grains (Kristensen et al. 2015; Wallinga 2002; Wallinga et al. 2019). Small-aliquot quartz OSL and single-grain feldspar luminescence advances the applicability of luminescence for studying mixing. Measuring the signal on individual grain level produces more meaningful results regarding mixing, as it also shows the fraction of reworked grains, and therefore the effectiveness or reworking (Reimann et al., 2017; Wallinga et al., 2019). Single grain luminescence has been successfully applied in terrestrial systems to determine effective bioturbation rates (Román-Sánchez et al., 2019) and has potential to quantify mixing by different bioturbation modes (van der Meij et al., 2025). Feldspar infrared stimulated luminescence (IRSL) or post-infra-red IRSL (pIRIR) measured at varying temperatures are commonly used single-grain signals. As these signals are less light sensitive than quartz OSL: they need longer light exposure to be fully reset and can therefore hold additional information on the transport and deposition history(e.g., Choi et al., 2024; de Boer et al., in review; Guyez et al., 2023).

Measuring single-grain luminescence signals with differential bleaching rates can inform about the light exposure duration and whether bleaching occurred under water (de Boer et al., in review). They can therefore be used to identify intertidal storm deposits (Pannozzo et al., 2023), or to infer whether bleaching occurred during subaqueous transport or during subaerial exposure on the tidal flat. Bleaching potential is low during storms and

strong hydrodynamic conditions, due to high turbidity and low light exposure, while biotic mixing also takes place
during calm conditions and intensifies in the summer season, when light and thus bleaching potential is higher.

140 Moreover, biotic mixing may occur during low tide, when the flat is subaerially exposed.

The goal of this study is to unravel the relative contributions of bioturbation and physical dynamics to sediment
mixing in a tidal flat environment, using tracers that act on different timescales and on different sediment fractions.
We compare traditional short-term (Chl-*a*, luminophores) and long-term (^{210}Pb) tracers and test the applicability
of single-grain luminescence as a bioturbation tracer for sand grains. We aim to answer the questions: (i) can

145 single-grain luminescence be meaningfully applied as a bioturbation tracer in such dynamic environments? And
(ii) how do short- and long-term tracers aid in distinguishing bioturbation from physical mixing? We hypothesise
that, if biotic mixing dominates, we will observe tracer-dependent mixing and, depending on the benthic
community, diffusive or advective transport. With intense bioturbation, the slow-to-bleach luminescence signals
will also be more fully bleached. If physical dynamics are responsible for the deposition and sediment mixing, we

150 expect a clearer stratification. Slow-to-bleach luminescence signals will be poorly bleached. We compare two
adjacent intertidal locations: a sandy and a muddy flat in the Dutch Wadden Sea.

2. Methodology

2.1 Site description

The sampling site is located in the western Dutch Wadden Sea, near the northern tip the island of Texel (Fig. 2).

155 We selected two adjacent intertidal locations: a muddy site (53'9.074N, 4'53.67E; -0.055 m relative to Dutch
ordinance datum (NAP)—approximately mean sea level), with visible benthic activity (small cast mounds,
burrows), and a sandy site (53'9.013N, 4'53.931E; 0.004 m), with presence of large lugworms (large cast mounds
and depressions). The sites are microtidal, with a mean tidal range of 1.43 m at the nearest measurement station
(Oudeschild). This implies that during high tide the maximum water depth is 0.7 m (0.8 m during spring tides).

160 The sites are located approximately 5 km south-eastwards of the tidal inlet and are relatively sheltered from the
prevailing south-westerly winds.
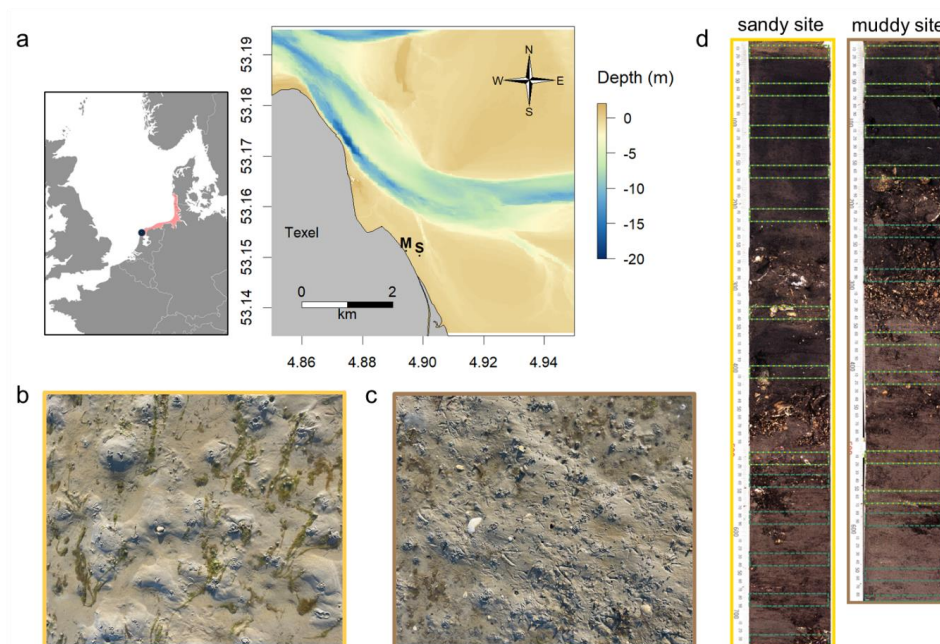
Figure 2: a. Map and bathymetry of the study area, located north-east off the island of Texel Wadden Sea (Netherlands), with muddy (M) and sandy (S) sampling locations indicated. The inset shows the location of the Wadden Sea (red) in western Europe, and the location of the study site (blue); picture of sediment surface at the sandy site (b) and muddy site (c); d. core scan from long cores from both sites, with the sampling intervals for ^{210}Pb (green) and luminescence (yellow) samples indicated.

2.2 Benthic community sampling and analysis

To describe the benthic community, we sampled both sites using a hand corer (surface area of 177 cm^2), which was pushed into the sediment until encountering the first shell layer. The core sample was sieved over 1 mm mesh size and the remaining coarse fraction including biota was conserved in 4 % formaldehyde, buffered with borax and stained with Rose Bengal (CAS Number: 4159-77-7). In the laboratory, samples were sorted and biota were identified. Next, dry weight (DW) was measured after drying at 60°C for 2-3 days and ash free dry weight (AFDW) was measured after combustion at 560°C for 5 hours, to yield biomass per taxon. Due to the limited depth of our samples, the resulting densities for *Arenicola marina*, were not consistent with the field observations of large *A. marina* casts at the sandy location. Therefore, we also derived *A. marina* density based on cast counts from pictures from both locations (4 pictures per site). To estimate individual biomass, we actively collected *A. marina* from both sites with a spade (N = 17), which were dried in the same way as the benthic community samples. We derived bioturbation traits and living depth from a trait database (Beauchard et al., 2023) and calculated the total biomass per trait group.

2.3 Sampling of long cores

Two replicate sediment cores were collected at each site in August 2023 for grain size analysis, geochemical composition (X-ray fluorescence, XRF), ^{210}Pb and luminescence analysis. The cores were obtained by hammering two PVC tubes (inner diameter 96 mm) side by side vertically into the tidal flat deposits. After extraction from the tidal flat, the cores were sealed and transported to a dark container where under subdued amber-light conditions a core slicer was used to split each core into two halves. One of the cores halves was kept for luminescence and ^{210}Pb sampling, the other was kept for XRF scanning and sediment composition. We subsampled luminescence and ^{210}Pb samples by cutting 25 mm thick slices from the top to the bottom of each core, of which we selected eight per core for luminescence analysis (see Fig. 2 and Table A1 for intervals). The inner portion of each slice was used for luminescence equivalent dose (D_e, Sect. 2.6.1) estimation and ^{210}Pb analysis, while the outer material was reserved for determining the environmental dose rate ($D°$, Sect. 2.6.2). The sediment was wet-sieved in a dark room environment to separate the grain-size range of 212–250 μm, used for luminescence analysis, from the fraction smaller than 63 μm, used for ^{210}Pb analysis. We measured ^{210}Pb for five additional samples of each core, amounting to a total of 13 ^{210}Pb samples per core.

2.4 Sediment composition: grain size and X-ray fluorescence (XRF)

For grain size distribution, half of each long core was subsampled in 25 mm slices. These samples were freeze-dried, sieved over 1000 μm and measured by laser diffraction (Mastersizer 2000, Malvern Instruments). We determined the volumetric content of sediment size fractions from mud to coarse sand, and the median grain size (d_{50}), and 10th and 90th percentile of the grain size distribution (d_{10} and d_{50}).

We measured bulk elemental composition over the entire depth of the long cores at 10 mm resolution by X-ray fluorescence, using an AvaaTech XRF core scanner at the Royal Netherlands Institute for Sea Research (NIOZ) (Richter et al., 2006). Each section was exposed for 10 s with a power supply of 10 kV/0.60 mA, or 30 kV/1.6 mA. This yielded bulk elemental composition as element intensities in total counts or counts per second. We selected the following elements and ratios as environmental proxies: Si:K (sand indicator), Cl:Fe (saline pore water indicator, thus proxy of porosity); Ca:Fe (shell content indicator; Croudace et al. (2006)), Rb (silt/clay mineral indicator; Guyard et al. (2007); note that the XRF detector window contains rubidium crystals, explaining high counts for this element); and Br (organic content indicator; Ziegler et al. (2008)).

2.5 ^{210}Pb measurement via alpha spectrometry

The downcore distribution of ^{210}Pb in the mud fraction (<63 μm) of the sediment was determined indirectly through alpha spectrometry measurement of its grandchild isotope ^{210}Po. To this end, 0.5 g of dried and homogenized mud, wet sieved from the bulk sediment sample, was spiked with 1 ml of a standard solution of ^{209}Po in 2 M HCl, and then leached for 6 h in 10 ml of concentrated HCl, heated in a hotblock to 85 °C. After diluting the fluid with 45 ml of Milli-Q water and adding 5 ml of an aqueous solution of ascorbic acid (40 g L^{-1}), natural ^{210}Po and added ^{209}Po were collected from the fluid by spontaneous electrochemical deposition on silver plates, with the fluid kept at 75 °C in a hotblock for 16 h. For subsequent alpha-spectrometry, Canberra Passivated implanted Planar Silicon detectors were used. ^{210}Pb activity was calculated from the measured ^{210}Po activity, assuming secular equilibrium and correcting for the time elapsed since collection of the samples.

2.6 Luminescence measurements

The luminescence samples were prepared at the Netherlands Centre for Luminescence Dating (NCL) under amber

220 light conditions.

2.6.1 Equivalent dose (D_e) measurements

Quartz and feldspar luminescence samples were prepared following a standardised protocol (Appendix A2.1). The multi-grain quartz aliquots (48 per sample) were measured using an automated Risø TL/OSL DA-15 reader, following a Single-Aliquot Regenerative-dose protocol (SAR) (Table 2). The single-grain feldspar measurements

225 were performed using an automated Risø TL/OSL DA-20 reader with an automated detection and stimulation head (DASH) and an EMCCD camera (Kook et al., 2015). A multiple-elevated-temperature (MET) pIRIR measurement protocol was used (Table 2) (de Boer et al. 2024a; Li & Li 2011). Three single-grain discs per sample were used, resulting in approximately 250 grains measured per sample. For more details on the measurement procedure, see Appendix A2.1.

230 **Table 2.** Luminescence measurement protocols: Single-Aliquot Regenerative-dose protocol (SAR) for multi-grain quartz measurements and multiple-elevated-temperature (MET) pIRIR measurements for single-grain feldspar.

#	Multi-grain quartz protocol	OSL signal	Single-grain feldspar protocol	Feldspar signal
1	Natural/ regenerative dose (Gy)		Natural/ regenerative dose (Gy)	
	(0, 7.3, 0, 7.3, 7.3)		(0, 1.4, 2.8, 5.6,11.3,0,1.4)	
2	Preheat at 200 °C (10 s)		Preheat at 200 °C (60 s)	
3	*IRSL at 30 °C (40 s)		IRSL at 50 °C (108 s)	IRSL-50 Li
4	OSL at 125 °C (20 s)	OSL-125 Li	IRSL at 175 °C °C (108 s)	IRSL-175 Li
5	Test dose (4.7 Gy)		Test dose (2.8 Gy)	
6	Preheat at 180 °C (10 s)		IRSL at 50 °C (108 s)	IRSL-50 Li
7	OSL at 125 °C (20 s)	OSL-125 Li	IRSL at 175 °C (108 s)	IRSL-175 Li
8	Bleach with OSL at 190 °C (40 s)		Hot bleach with IR-LEDs at 210 °C (108 s)	

*Only in the last regenerative run to check for feldspar contamination

2.6.2 Dose rate ($D°$) measurements

Environmental dose rates, the natural amount of natural ionizing radiation absorbed by a sample per unit of time,

235 were determined with gamma-ray spectrometry (Appendix A2.2). Results are combined with information on burial history, water and organic content history, and the measured grain-size fraction to calculate the effective external beta and gamma dose rates (Cunningham et al., 2022). For cosmic dose rate calculation (Prescott et al., 1994), we assumed gradual burial of the samples to the present depth. Per core, the average water content over all samples was used, yielding gravimetric water content of 28.5 % (muddy core) and 25.5 % (sandy core), with a

240 relative uncertainty of 25 % to account for variations over time. The organic content per sample was used to account for attenuation. We included an internal alpha dose of 0.010 ± 0.005 Gy ka^{-1} for quartz (Vandenberghe et al., 2008) and 0.050 ± 0.025 Gy ka^{-1} for feldspar (Kars et al., 2012). An internal K-content of 12.5 % was assumed for the K-feldspar grains. As gamma-rays penetrate 20–30 cm in the deposits, contributions from adjacent layers are accounted for following the approach of Wallinga et al. (2010).

2.6.3 Data analysis

The sample age is calculated by dividing the equivalent dose value by the mean dose rate: age (years) = D_e (Gy) / $D°$ (Gy year^{-1}) (Rhodes, 2011). To interpret the quartz OSL single-aliquot (multi-grain) and feldspar IRSL and pIRIR single-grain age distributions, we used several approaches. Firstly, a mean was calculated after iterative removal of datapoints that deviate more than two standard deviations from the mean. This iterative approach aims to identify the mean age, while minimising bias due to outliers that may be caused due to poor bleaching or recent input of young (bleached) grains. Secondly, a logged version of the Central Age Model (CAM) (Galbraith et al., 1999) was used to quantify the overdispersion and obtain a mean burial age for samples that are relatively well-bleached. Finally, the logged bootstrapped Minimum Age Model (bMAM) (Cunningham & Wallinga 2012; Galbraith et al. 1999) with a sigma-b of 0.25 ± 0.05 was used to determine the absorbed dose of the youngest population of grains. Lastly, we determined the interquartile range (IQR) of the age distribution of each signal, as a direct metric of the width of the distribution for each signal (van der Meij et al., 2025). All analyses were performed in R (R Core Team, 2024) with use of the Luminescence package (Kreutzer et al., 2025).

2.7 Luminophore tracer experiment

Simultaneous to the long core sampling, we started a luminophore tracer experiment adjacent to both sampling locations. Fluorescent coated luminophores (red/pink tracer, size range: 0–125 μm) were mixed with sieved native sediment from each site (ratio 1:10 for the muddy sediment and 1:17 for the sandy sediment) and applied to the sediment surface as 15x15x0.5 cm frozen tiles. Per site, three experimental plots were created by aligning four of these tiles—thus each covering a total area of 30x30 cm. These were sampled on day 2, 16 and 30 by pushing a PVC tube (diameter 36 mm) at least 20 cm deep into the sediment. The sediment cores were frozen upright. For analysis, the frozen cores were sliced in length direction with a tile saw. The cutting surface was scraped clean in lateral direction until the still frozen sediment was reached. If cutting had resulted in visible artefacts in the sediment (cavities or disturbed sediment surface), the damaged core or half core was excluded from analysis. Next, both halves of the core were photographed in a dark room under ultraviolet light, with a ruler for scale reference. The images were processed using ImageJ (Schneider et al., 2012): first, we adjusted the display settings Level ≈ 50 and Window ≈ 100. Red and orange pixels were then identified per 2-cm depth slice by extracting RGB values of each pixel, and applying thresholds (R > 150, G > 40, G < R - 30, B < 100). The total count of pixels meeting these criteria was recorded as the red–orange pixel count. The average number of pixels per depth interval were averaged over both core halves.

2.8 Chlorophyll-*a* sampling and measurements

Chlorophyll-*a* cores were collected next to the luminophore tracer experiment. Cores (inner diameter 36 mm) were collected on August 22nd and October 5th, 2023 (day 1 and day 45 of the luminophore experiment). The cores were pushed into the sediment as deep as possible, or at least 15 cm deep. We sliced the cores every 0.5 cm down to 3 cm depth, then every 1 cm down to 15 cm depth. The samples were stored at -80 °C and freeze-dried for 72 hours before analysis. Next, we homogenised and weighed an aliquot of the sediment (approximately 1000–1500 mg for the sandy site samples and 300–500 mg for the muddy site samples). We extracted Chl-*a* by adding 5 ml 90 % acetone in 50 ml centrifuge tubes and running them in a bullet blender (BB50-AUCE, Next Advance) for 15 min, after which 5 ml 90 % acetone was added again and extraction was repeated for another 15 min. The

extracts were measured in a spectrophotometer (Specord 210, Analytik Jena) at 630, 647, 664, 665 and 750 nm. From the measured extinction values, we calculated Chl-*a* concentration following Ritchie (2006).

285 ## 3. Results

3.1 Benthic community

Macrozoobenthic community biomass and abundance were higher on the muddy site (approximately 19 g AFDW m^{-2}) than on the sandy site (3.8 g m^{-2}; Appendix A3, Table A2). Both locations contained a large fraction of taxa which could be classified as biodiffusers (Appendix A3, Fig. A1). The sandy site contained a larger fraction of

290 downward conveyors, while more upward conveyors inhabited the muddy site. Density of downward conveying lugworms (*A. marina*) was higher on the muddy site (98 ± 42 individuals m^{-2} versus 44 ± 11 individuals m^{-2} on the sandy site), while worms were larger on the sandy site (0.16 g individual^{-1} versus 0.05 g individual^{-1} on the muddy site). We estimate total *A. marina* biomass therefore to be slightly higher on the sandy site (6.9 g AFDW m^{-2} versus 5.1 g AFDW m^{-2}), and to form a substantial part (approximately 60 %) of the total biomass at the sandy

295 site, compared to 20 % at the muddy site.

3.2 Sediment composition and grain size

On the sandy site, the top ~0.3 m of the sediment consists mainly of fine sand, with a mud content under 10 % (Fig. 3a). From here, the coarse sand fraction gradually increases to ~40 % at a depth of 0.45 m. Below 0.45 m, the sediment is less well-sorted, containing both a 20–40 % mud fraction, as well as coarse and very coarse sand

300 and a variable d_{90} (Fig. 3b) We observed shell layers between 0.27–0.29 and 0.44–0.47 m, also reflected in increased Ca:Fe ratios from the XRF measurements. Below the second shell layer, the marine pore water (Cl:Fe) decreases and organic matter content (based on the Br indicator) increases (Fig. 3e-i).

At the muddy site, the top 0.15–0.20 m of the sediment is less well sorted: a large mud fraction (10–25 %), as well as a substantial fine and medium sand fraction are present (Fig. 3c, d). A shell layer was present between

305 0.18–0.34 m. Between 0.2–0.45 m, some layers contain coarse particles (500–1000 µm), which is also reflected in peaks in d_{90}. The amount of marine pore water (Cl:Fe) slightly increases downcore, whereas sand content (Si:K), mud content (Rb) and organic matter (Br) remain relatively constant (Fig. 3j-n). A brick present in the shell layer gives evidence of anthropogenic influence and suggests a relatively young deposit.
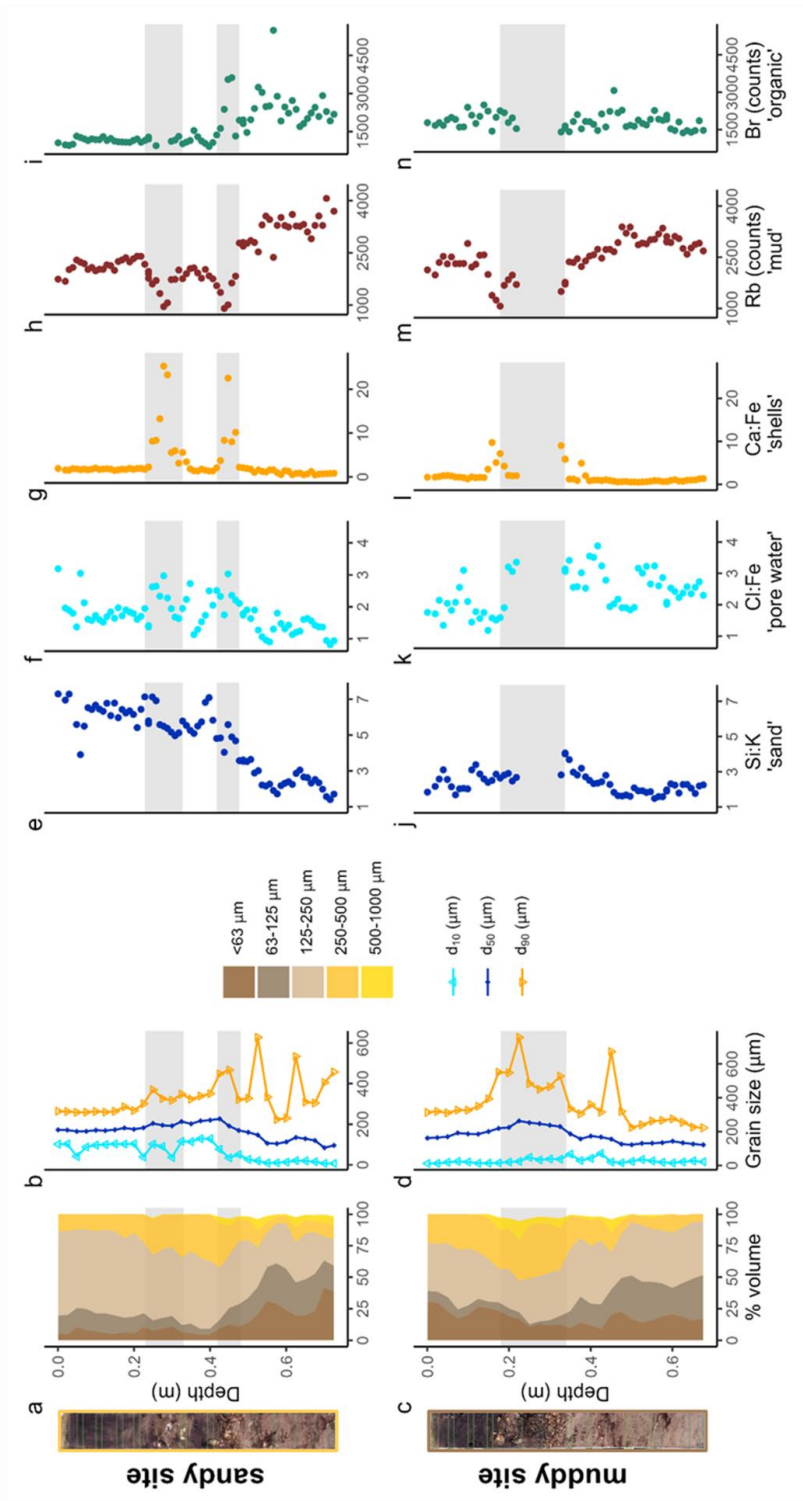
Figure 3: Sediment composition at the sandy site (top) and muddy site (bottom): stacked grain size fractions (a, c); d_{10}, d_{50} and d_{90} (b, d); elemental composition (e–n): Si:K, higher ratios indicate sand; Cl:Fe, higher ratios indicate marine pore water; Ca:Fe, higher ratios indicate shells; Rb counts representative of silt and clay, and Br counts, representative of organic matter. Note that the cumulative grain size fractions (a, c) do not amount to 100 % when coarse >1000 μm material was present. The data gap in the mud cores (j–n) resulted from a scanning failure due to the presence of a brick. Grey bands show the shell layers. The core scans are shown left of the figure.

310
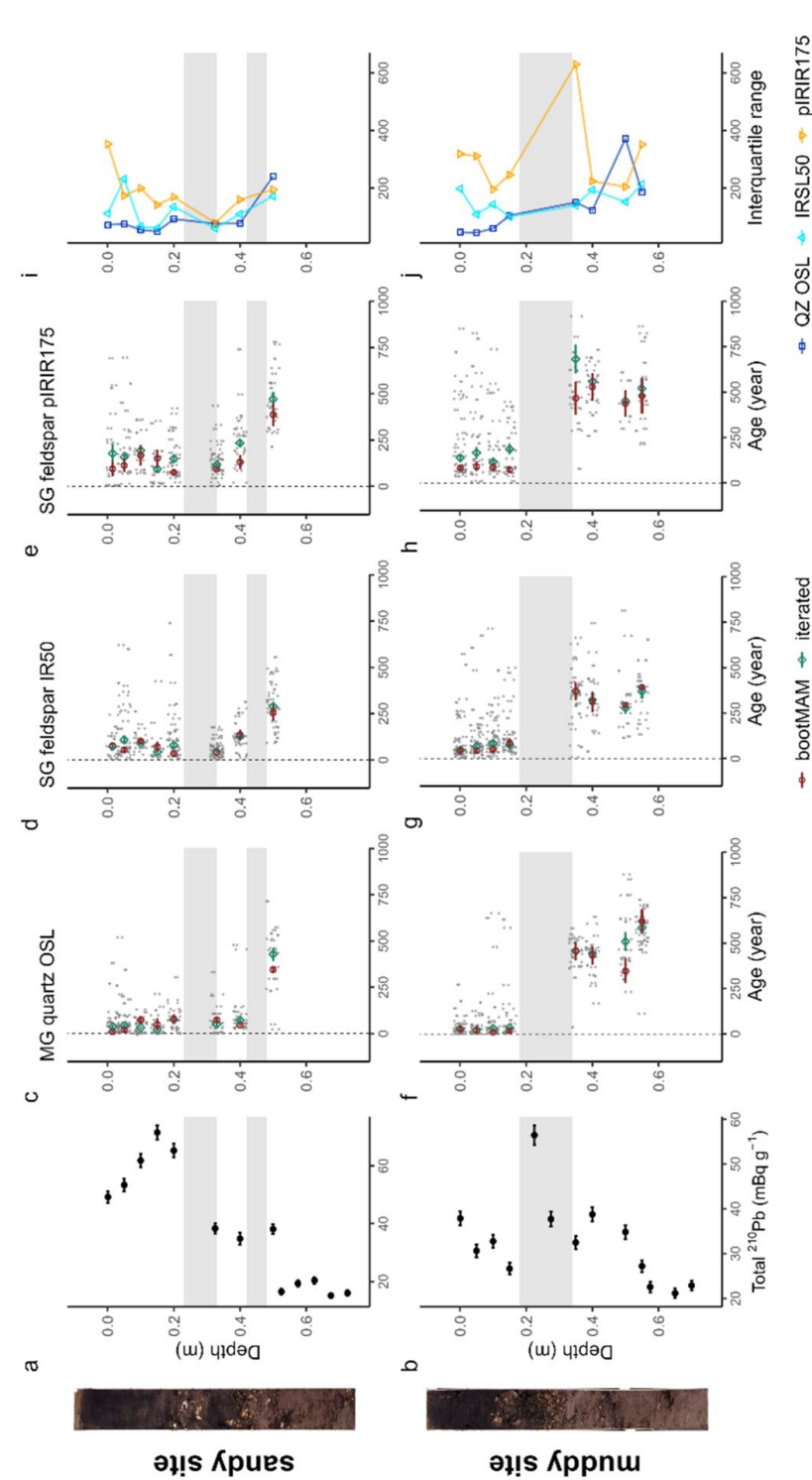
Figure 4: Tracer profiles from ^{210}Pb (a, b) and luminescence signals, with the single-aliquot or single-grain data jittered in grey and green and red markers indicating the modelled iterated or bootMAM age with standard error (c-h); interquartile range of luminescence age distribution (i, j) for the sandy (top) and muddy site (bottom). Grey bands indicate the shell layers. The core scans are shown left of the figure.

2.3 Long-term tracers: ^{210}Pb and luminescence profiles

Above the first shell layer at the sandy site, ^{210}Pb activity was lowest in the surface slice (0–0.025 m depth), and increased to a subsurface peak at 0.15 m (Fig. 4a). Below the first shell layer (<0.29 m), activity decreased, to a nearly constant level below 0.5 m. At the muddy site, ^{210}Pb activity slightly decreases down to 0.15 m, peaked in
315   the first shell layer at 0.225 m (Fig. 4b). Until down to 0.4 m, below the second shell layer, ^{210}Pb activity remained high. Activity then decreased to an apparently constant level of ~22 mBq g^{-1} between 0.5–0.6 m.

In discussing the luminescence ages, we focus on the quartz OSL ages obtained through the iterated age model, as this provides the best estimate of the last light exposure of the majority of the grains. Quartz bootMAM ages indicate the last time of introduction of light exposed grains through bioturbation. For feldspar, heterogeneous
320   bleaching is to be expected and therefore we focus on the interquartile range of the age distribution and bootMAM derived ages to infer information on light exposure and thus process information.

The quartz OSL iterated ages suggest last light exposure well within the past 100 years for sediments within the top 0.4 m at the sandy site (Fig. 4c) and 0.15 at the muddy site (Fig. 3i) (Appendix A4, Table A3a). A jump in age is observed between the samples at 0.4 and 0.5 depth at the sandy site, with an age of 430 ± 40 years for the
325   latter according to the iterated model. For the muddy site, older ages (440 ± 30 to 640 ± 40 years) were obtained for the part below the shell layer.

The feldspar IR50 and especially the pIRIR175 signals were not fully bleached in a large fraction of the grains in the top 0.2 m of both cores. At the sandy site, grains with a low pIRIR175 age were only present at 0, 0.15 and 0.325 m; at the muddy site such young grains could be identified at 0.05 and 0.15 m. The ages obtained using the
330   bootMAM approach on the IR50 signal tend to be a few decades older than those obtained through quartz OSL iterated mean, while bootMAM derived pIRIR175 ages are significantly older (typically by a few centuries, Table A3b, c). An exception is formed by the samples from the deeper parts, where IR50 results tend to be younger than quartz OSL, while pIRIR175 agree with quartz OSL. The single-grain age distributions obtained on both feldspar signals are also broader than those obtained through quartz OSL.

335   ### 2.4 Short-term tracers: Chlorophyll-*a* and luminophore profiles

Both short-term tracers show a high spatial variability. Whereas two muddy cores and one sandy core contained sub-surface maxima of Chl-*a* concentration (Fig. 5a, b; at 3, 15 and 6–8 cm depth respectively), in the other cores the Chl-*a* concentration showed a more exponential decrease with depth. At the bottom of the cores in all sites, still some Chl-*a* was present above the analytical detection limit (0.2 μg g^{-1}), which could indicate the supply of
340   Chl-*a* younger less than 3 months ago, or reflect Chl-*a* adsorption to sediment.

Luminophores were already worked down to 18 cm (sandy site) and 20 cm (muddy site) within 2 days (36 hours) after initiation of the experiment (Fig. 5c, d). In these cores, the reworking could be clearly linked to bioturbation, as two bivalves were found in the cores with increased luminophore concentration around their burrows (Appendix A5, Fig. A2; *Scrobicularia plana* at the sandy site and *Cerastoderma edule* at the muddy site). Similar
345   high subsurface luminophore concentrations were not observed in the cores collected at later time points, although some luminophores could be found at greater depths. We saw similar between-core and thus spatial variability as in the Chl-*a* measurement.
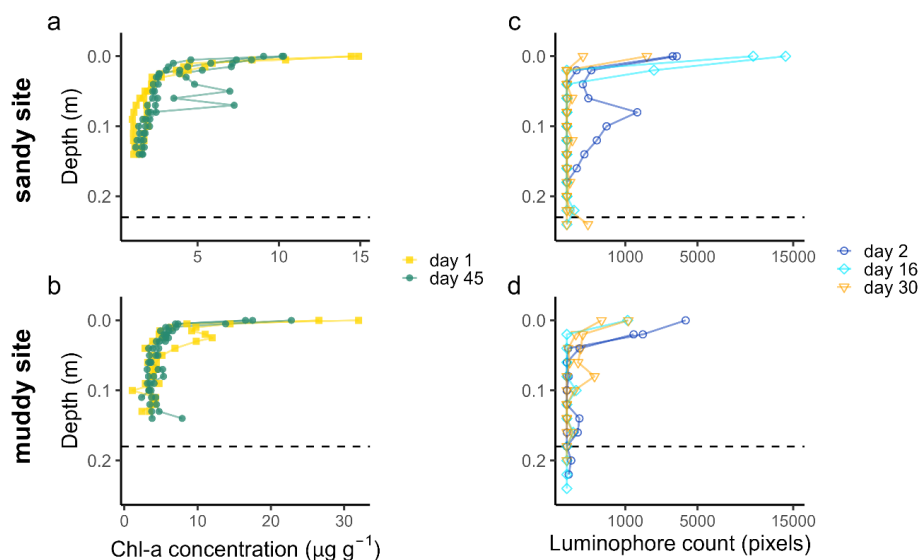
350

Figure 5: Chlorophyll-*a* (a, b) and luminophore (c, d) profiles from the sandy site (top) and muddy site (bottom), sampled at different time points (day, starting from August 21st, 2023). Note that the x-axis of the luminophore plots was square-root-transformed to increase the visibility of low pixel counts. The dashed line indicates the depth of the top of the shell layer, as determined from the deep cores.

4. Discussion

355

The signal-depth profiles were tracer-dependent. We observed subsurface maxima of Chl-*a* and luminophores on both the sandy and the muddy site down to a depth of 0.15–0.25 m. This rapid translocation of young particles to depths of 0.15–0.25 m also showed in the ^{210}Pb profiles and to some extent in the feldspar pIR175 luminescence profiles. The quartz and feldspar IR50 luminescence results rather suggested that at least the top 0.15–0.2 m of

360 the sediment was deposited recently, hampering identification of even younger sand grains mixed in through bioturbation. The slow-to-bleach feldspar signals were not fully reset in the top layer, although some input of young grains to deeper layers could be identified. This suggests episodic deposition of the top layers, or insufficient mixing to expose all grains long enough to unfiltered light. In what follows, we will provide a combined interpretation of what these results tell about deposition and mixing processes in dynamic intertidal

365 environments.

4.1 Worms or storms?

In the sediment composition, we did not observe any clear layering in the top decimetres of sediment at both sites which could be attributed to storm deposition. This may be due to an overly coarse vertical sampling resolution, even though our resolution of 25 mm should have been sufficient to capture storm deposited layers, which can

370 have a thickness of centimetres (Zhou et al., 2022). At the sandy site the top of the profile was relatively homogeneous. The top decimetres of the sandy core also appeared to be better sorted than the top part of the

muddy core (Fig. 3a-d). Generally, hydrodynamic reworking would be expected to result in more uniformly sorted sediment, whereas biota can create localised patches of finer or coarser material (Aller & Cochran 2019; Bentley & Nittrouer 2012) thus resulting in variable sorting of individual sediment samples (Rhoads & Stanley 1965).

375 Furthermore, the presence of shell layers may indicate biotic influence, since bioturbators such as *A. marina* are unable to ingest coarse particles like shells, which then remain at the feeding depth (Reise 2002; van Straaten 1952), while the ingested sand will be deposited on the sediment surface and subsequently mixed into the sediment.

The tracers targeting the fine-grained sediment fraction showed clear signs of bioturbation. During the

380 luminophore experiment, no storms or strong winds occurred, therefore vertical luminophore displacements can solely be attributed to bioturbation. Both the short-term (luminophores and Chl-*a*) and the long-term (^{210}Pb) tracers showed sub-surface peaks, illustrating that advective vertical transport of particles occurred. This is coherent with the observed macrozoobenthic species that are known non-local mixers (see Sect. 4.3). In addition, the gradual vertical gradients of ^{210}Pb, and of Chl-*a* till 0.15–0.2 m point to substantial diffusive bioturbation in the top

385 decimetres of the sediment, or rapid deposition within the previous months.

The luminescence data gives more details on the deposition and reworking of sand grains. The narrow age distributions obtained through quartz OSL indicate that this signal was well-bleached. The bootMAM and iterated age estimates are very similar, both likely reflecting the time of deposition. The narrow distributions in the top layer (0.4 m at the sandy site and 0.15 m at the muddy site) imply that the vast majority of grains were recently

390 (within the past few decades) exposed to sufficient light to fully reset quartz OSL signals. However, the older ages obtained through feldspar IRSL, even for the relatively fast bleaching IR50 signal, indicate that for a large fraction of grains, full light exposure during and after deposition was limited. Especially old (>500 years) pIRIR175 measurements in the top 0.10 m at both sites indicate that light exposure prior to burial was insufficient to bleach this signal. It is less likely that these grains are worked upwards by bioturbators from deeper deposits, as other

395 grains of this age were only found below the shell layer at 0.35–0.5 m depth. Both feldspar signals from the top decimetres were not as homogeneously bleached as would be expected with intensive reworking. We conclude that the luminescence ages primarily reflect the time of deposition, with quartz OSL providing most reliable depositional ages. The feldspar IRSL and pIRIR results also indicate burial age but are overestimated due to incomplete resetting of these signals upon deposition and burial.

400 The luminescence signals gave a few hints of bioturbation as well. Firstly, at both sites, young grains with nearly fully bleached pIRIR175 signals are present at larger depths. At the sandy site, such young grains can be found at 0.15 m, coinciding with the subsurface ^{210}Pb peak. At the muddy site, the young grains are only present above the shell layer, at 0.05 and 0.15 m. This could point at the advective transport of young sand grains to this depth, or good bleaching conditions during deposition of these layers. Given the combination of bioturbation evidence from

405 the other tracers, and the lack of sedimentary structures, we deem bioturbation to be the most likely process. Secondly, feldspar signals in the very top layer (0–0.05 m) at both sites were less well bleached and had wider distributions than those at 0.1–0.2 m deep. Possibly, grains that are recently deposited under low bleaching conditions and are buried close to the surface, are not always directly resurfaced by bioturbators. These grains require a longer period of bioturbation to be bleached further. This hypothesis is supported by Bentley et al.

410 (2014), who described a shallow (1–4 cm) stratified top layer, which was not yet bioturbated, above a more intensely bioturbated zone in a muddy intertidal environment. Secondly, the luminescence data provides some

evidence for exchange of grains between stratigraphic layers of different depositional age. Some grains in the luminescence age distribution had ages similar to those of the underlying deposit, even if a shell layer is present in between. At the muddy site, a high level of ^{210}Pb was also present in and below the shell layer. From these observations combined, we conclude that transport of fine particles can sometimes extend beyond the shell layer. Madsen et al. (2011) also reported quartz OSL profiles on an intertidal flat and attributed a change in apparent sedimentation rate to bioturbation. Their site was not very dynamic, and bioturbation was more likely to be the main mixing process present. The combined evidence of small aliquot quartz OSL and single grain feldspar IRSL50 and pIRIR175 suggests that deposition at our site was episodic and that bioturbation was less efficient in bleaching these signals by resurfacing the grains. Furthermore, given that deposition was recent, it is not possible to clearly differentiate bioturbated grains from those grains that were last light-exposed prior to deposition as is done in terrestrial soils (e.g., Reimann et al. (2017)). Hence, we cannot deduce bioturbation rates from our data using approaches as suggested by van der Meij et al. (2025).

4.2 Age gaps and sedimentation rates

We could not derive sediment accumulation rates, because our combined signals pointed to a combination of sediment mixing and episodic deposition. Therefore, assuming the age-depth profiles to be the result of gradual sedimentation alone would be incorrect in this dynamic environment. Quartz OSL showed a hiatus in age between the top and the middle part of the core at the muddy site but not at the sandy site, while ^{210}Pb also indicated a hiatus in activity at the muddy site only (Fig. 4a). Such age gaps can be caused by erosion followed by rapid accumulation, mounding by bioturbators (Kristensen et al., 2015; van der Meij et al., 2025), or switching between a depositional and an erosional regime with bioturbation penetrating the older deposits (Madsen et al., 2011). The opposing gaps of the radionuclide and luminescence tracer profiles could be an effect of an age underestimation of ^{210}Pb compared to OSL of older sediments (Madsen et al., 2007). However, the ^{210}Pb activity just below the shell layer in the muddy site is too high to be fully explained by such an inaccuracy. Instead, we expect differential transport of fine and coarse particles through the shell layer to play a role.

Combining the information from luminescence signals, deposit composition and ^{210}Pb, we propose the following possible scenarios for sedimentation history (Fig. 6):

- On the sandy site, rapid sediment deposition took place approximately 400 years ago. The original sediment surface was covered with a new thick layer of sand, and the benthic fauna recolonised the new layer. The quartz signals in this new deposit were then uniformly bleached by bioturbation and physical resuspension and deposition, although incidentally some grains were still exchanged with the bottom layer. Through bioturbation, also the first shell layer was formed. Recently (<100 years ago) another large, rapid deposition event happened. This shifted the bioturbation depth upwards, forming a new shell layer higher up. Still some fines (^{210}Pb) moved downward through the shell layers, but most accumulated on feeding depth of bioturbators.

- On the muddy site, the top 0.2 m of sediment were gradually deposited, starting approximately 500 years ago. The layer that is now at 0.35 m then fell below the bioturbation depth and was not any longer exposed to light. The sediment has then slowly been accumulating with bioturbation resulting in bleached OSL signals and the formation of a gradually thickening shell layer. Elevated ^{210}Pb activity below the shell layer could be due to passive infiltration of fines through the porous shell layer. The strong break in luminescence age

suggests little exchange of sand grains through the shell layer, and thus differential displacement of coarse and fine particles.
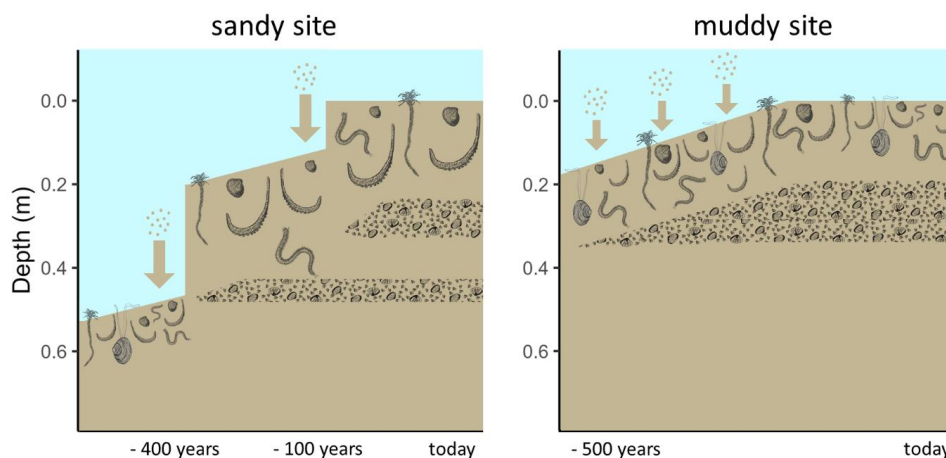
Figure 6: Conceptual diagram of sedimentation history scenarios of the sandy (left) and muddy (right) site.
455   Larger arrows represent more rapid sedimentation. The depth represents the current depth in the cores. Shell layers and benthic community are represented schematically with a lower species abundance and biomass, but larger lugworms (*Arenicola marina*) on the sandy compared to the muddy site.

4.3 Differences between sites: hydrodynamics and community type?

The sandy site was relatively more exposed to energetic hydrodynamic conditions than the muddy site. This may
460   have caused the surprisingly low surface ^{210}Pb activity, as waves and tidal currents may resuspend and wash away the recently settled ^{210}Pb-rich material at each tide. The Chl-*a* concentrations were also lower at the sandy site than on the muddy site, but this might be due to differences in degradation rates of Chl-*a* (Sun et al., 1993). The bleaching potential of the luminescence signals could differ between the muddy and sandy tidal flats (Pannozzo et al., 2023). When submerged, higher loads of suspended sediment will decrease subaqueous light penetration
465   during transport and (re)deposition on the muddy site (de Boer et al., in review). The sandy site is more elevated and therefore slightly more often exposed to subaerial bleaching than the muddy site due to its lower inundation times. These differences in bleaching potential and probability may have resulted in the lesser bleaching and wider distributions (Fig. 4j) of the luminescence signals on the muddy site.

The sandy and muddy site also differed with respect to the density, biomass and composition of the benthic
470   community. The muddy site contained a relatively higher abundance and biomass of taxa that could be classified as biodiffusers and surficial modifiers. This leads to a higher contribution of diffusive mixing and could also partly explain the larger interquartile ranges of the luminescence signals at the muddy site, compared to more effective bleaching through advective vertical bioturbation at the sandy site (van der Meij et al., 2025). Subsurface maxima of fine-grained tracers, pointing to advective transport, were more pronounced in the sandy site. One of the main
475   likely bioturbating agents was conveyor-belt reworking polychaete *A. marina*. While the muddy site contained a higher density of small individuals, this species comprised only a fifth of the biomass here. The sandy site was

inhibited by fewer, but larger lugworms, so that this species was dominant in biomass here. Such large individuals live in 0.2–0.4 m deep burrows and often dominate sedimentary processes at sandy intertidal flats. Their presence leads to 4-400 times more likely particle reworking rates and an estimated full overturning of a 0.1–0.6 m layer

480   of sediment per year (Cadee 1976; Riisgård & Banta 1998; Volkenborn et al. 2007a). These lugworms were probably responsible for the subsurface accumulations of ^{210}Pb at feeding depth, as the ^{210}Pb-rich organic material is filtered from the ingested sand (Longbottom, 1970).

Other bioturbators might also have contributed to non-local transport of fine tracers at both sites. Ragworms (family Nereididae), such as *Hediste diversicolor*, were present at both sites. These worms build a gallery network

485   and can cause diffusive mixing of the surface layer, and advective downward transport, accumulating particles at the lower end of the gallery network due to passive sloping, burrow infilling and during rapid retraction (Foster-Smith 1978; Herringshaw et al. 2010; Ouellette et al. 2004). Another group that we deem responsible for non-local transport of fines are tentaculate polychaetes, which enhance fine particle transport from the water column into the sediment (Frithsen & Doering 1986). *Pygospio elegans*, a tube-building worm present in high densities

490   at both sites, constructs tubes 0.15 m into the sediment, and enhance transport of fine particles down to 3–5 cm depth (Bolam & Fernandes 2003). *Lanice conchilega* feeds on organic particles from the sediment surface or the water column and builds long tubes, down to 0.3–0.4 m into the sediment (Carey, 1987). Although this species was only present in the benthos core sample at the muddy site, we observed their tube endings, indicating their presence, on the sediment surface at both locations (Fig. 2b, c).

495   *Scrobicularia plana* is described as a surficial modifier in trait databases (Queirós et al., 2013). We however observed that this species also contributes to non-local mixing, as evidenced by luminophores that had moved rapidly to the living depth of this bivalve (Fig. A2). Similar discrepancies between 'theoretical' bioturbation traits and field observations were reported by (Morys et al., 2017). Therefore, a single trait-based community index for bioturbation (such as BP$_c$), could potentially be informative on larger spatial scales when a more extensive dataset

500   is available, but such an index may be less relevant for a local study.

4.4 Why are results tracer-dependent?

The differences between tracers are likely the result of particle size-specific physical and biological sorting mechanisms. Fine particles are more easily eroded and transported from the sediment surface by currents and waves. They are therefore less prone to remain on the surface for a prolonged period, whereas coarser sand grains

505   are more stable on the sediment surface. Fines are also more likely to move down into the sediment matrix by passive as well as active processes. In sandy, permeable sediments, fine particles can infiltrate with pore water flux (reviewed by Huettel et al. (2014)). Above that, fine and organic particles are more often selected by bioturbators, after which they may accumulate in deeper layers of the deposit. This particle selectivity is common among benthic taxa (Self & Jumars 1988).

510   Although the grain size range we selected for luminescence measurements (212–250 μm) falls outside of the feeding range of many polychaetes (Jumars et al., 2015), *A. marina*, expected to be a dominant bioturbator especially on our sandy site, does feed non-selectively on sediment particles below a size of 1000 μm (Baumfalk, 1979). Bioturbation of this species was shown to still result in accumulations of finer (130 μm) as well as coarser (500–1000 μm) particles at its feeding depth (0.1–0.14 m) (Gebhardt & Forster 2018). Bivalves can also exhibit

515   size- and particle-type specific selection, but this usually takes place post-capture (reviewed by Ward and

Shumway (2004)). Their burrowing movements rather than their feeding activity may thus vertically displace sand grains. *A. marina* as well as bivalves are therefore expected to have reworked sand grains and affected the luminescence tracer profiles.

520 It has been demonstrated that benthic fauna select for particle quality as well and prefer organic over inorganic particles (Taghon, 1982). Although we saw some advective transport of luminophores (Fig. 5c, d; Fig. A2), we did indeed not observe large sub-surface accumulation over time. One explanation might be that these inorganic particles do not accumulate at the organism's feeding depth in the same way as the organic matter-associated tracers that are retained in the digestive system. This is contrary to Gerino et al. (1998), who observed subsurface peaks of luminophores after 15 days, and additionally modelled Chl-*a* subsurface mixing rates to be in the same

525 order of magnitude as the mixing of non-organic particles in a shallow, muddy environment. In our dynamic intertidal environment, luminophores might have more easily eroded from the sediment surface, resulting in a decrease in surface supply over time, which possibly underlies the lack of later subsurface accumulations (Fig. A3).

A tracer can give meaningful information on mixing processes when the timescale of a tracer (e.g., radionuclide

530 decay rate) matches the timescale of the mixing rate: the longer the tracer timescale, the more particle displacements will have contributed to the signal distribution (Meysman et al., 2003). The luminescence signal is of a different nature than that of radionuclides, as it builds up after burial but resets at each sufficiently long or intense light exposure, rather than gradually declining over a known time. Signals that are more difficult to bleach (e.g. feldspar pIRIR175) require more light exposure to be reset compared to fast bleaching signals (e.g. quartz

535 OSL). They thus require a higher frequency of reworking events to be fully bleached. If sediments are however too young or intensely mixed, no recently reworked grains can be distinguished, as the sediment will be uniformly bleached. Under the conditions at our intertidal study sites, only the feldspar IR50 and pIRIR175 bleached slowly enough to be not fully reset during deposition or by bioturbation. Therefore, these signals can show subsurface supply of young sand grains (Fig. 4e, h) and incomplete bleaching during deposition (Fig. 4d, e, g, h). In this

540 relatively young and more intensely reworked sediment, where no 'old', never-mixed, sediment fraction appeared to be present, single-grain level measurements cannot be used for determining the bioturbation effectiveness (Reimann et al., 2017). Spatial scale also plays a role, especially for the short-term tracers. The small sampling surface of the Chl-*a* and luminophore cores and the patchy distribution of macrozoobenthos resulted in high variability between cores.

545 **4.5 Which tracer to use when?**

A combination of tracers best represents the intricate reality of physical and biotic sediment mixing processes. This corroborates Gerino et al. (1998), who showed that to accurately model bioturbation modes, measurements of multiple tracers with different characteristics are required. A multi-tracer experiment is however time- and resource intensive. Therefore, we propose a framework for deciding on the type of tracer to use, depending on the

550 research question at hand (Fig. 7). The process timescale, grain size fraction of interest and spatial density need to be considered. Depending on the rate and dominant mode of bioturbation, a short- or long-term tracer may be more appropriate (Lecroart et al. 2010; Meysman et al. 2010). Also, the potential targeting of organic food particles (e.g., Chl-*a*, ^{210}Pb) may be considered. Furthermore, the physical conditions at the field site determine the suitability of a tracer. If the field site is erosive or exposed to higher dynamics, fine luminophores might not

555   be representative over a longer period. With low reworking or light exposure (e.g., long inundation and turbid water), hard-to bleach luminescence signals are less likely to be bleached by bioturbation.
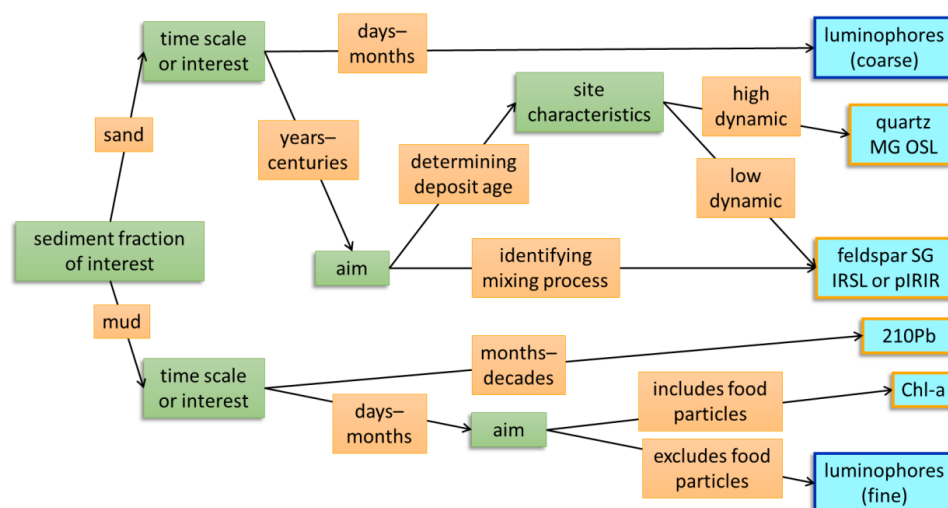
Figure 7: A decision tree for choosing the appropriate tracer type to identifying sediment reworking in intertidal environments. Green boxes indicate the attributes of the research question at hand that should be considered and

560   orange boxes show the possible responses, ultimately leading to the most suitable tracer (light blue boxes). The blue-outlined tracers are particles that actively need to be introduced in a natural system, while the orange-outlined tracers are native in intertidal sediments.

4.6 Outlook and implication

Feldspar single-grain luminescence is a promising tracer for deposition and mixing processes in intertidal

565   environments. Even though luminescence signals at our study sites pointed to high dynamics and rapid deposition, rather than being all fully bleached by bioturbation, they did give more information on long-term deposition and reworking of sand grains than other existing tracers can. We recommend testing this method in a less dynamic setting, where bioturbation dominates reworking, to improve interpretation of luminescence profiles and further explain the limited feldspar bleaching that we observed. The aim of this research was a qualitative rather than a

570   quantitative description of mixing processes. Given the young age of the sediments and the dynamics of the environment, a quantification of bioturbation as attempted by van der Meij et al. (2025) may be challenging. Nevertheless, single-grain and slow-to-bleach luminescence signals are a promising tool to further test and develop, for ultimately deriving bioturbation rates of sand grains in intertidal settings.

Our results highlight differences between the behaviour and bioturbation of sand and mud within the sediment

575   matrix. This distinction matters for stratigraphy: fines are more mobile within the sediment column, while sand grains have greater potential to preserve layered bedding. Although bioturbation is often assumed to homogenise stratigraphic records (Wheatcroft, 1990), our feldspar results suggest that the sand fraction is not intensively reworked. We also observed exchange of particles through the shell layer, suggesting that such layers do not necessarily form a hard boundary for bioturbators. Furthermore, the grain size-specific reworking can inform

580   process-based sediment transport models that quantify the mixing of specific sediment fractions within the bed
       (e.g., Armanini, 1995). Bioturbation increases the exchange of particles between the active (transportable) and
       substrate layer of the sediment, with higher exchange probability for small than for large particles.

       These findings also bear ecological implications. Fine, organic-rich tracers were rapidly carried below the aerobic
       zone and accumulated at depth, whereas young sand grains were not. This indicates that bioturbation affects
585   reactive compounds more strongly than coarse particles. Its influence on sand transport may thus be smaller than
       its role in sediment biogeochemistry and carbon storage. By modifying sediment mud content, bioturbators can
       modify their own habitat conditions. In sandy sediments, preferential reworking of fines can increase subsurface
       mud content. Such 'muddification' by cockles was demonstrated in a flume experiment (Soissons et al., 2019)
       and by *Ensis leei* in a field experiment (Witbaard et al., 2017). On the other hand, resurfaced fines may be
590   mobilised from muddy sediments, decreasing the sediment mud content (Montserrat et al. 2009; Volkenborn et
       al. 2007b; Wendelboe et al. 2013). These two-way processes affect large-scale intertidal flat morphology and
       sediment composition (e.g., Brückner et al., 2021; Le Hir et al., 2007). Finally, the integrated contribution of
       bioturbation and storms may be comparable when event energy and frequency are considered together. Whereas
       bioturbation is a continuous process of small particle displacements, storms are infrequent, but high energy events
595   (Fig. 1b). In effect, benthic animals influence daily sediment properties, while storm events 'reset' the system.
       Because most species have a relatively wide sediment tolerance (Kooistra et al., 2025), such episodic resetting
       does not necessarily result in a major community shift, and during calmer periods, bioturbators can once again
       modify sediments at smaller scales, potentially enhancing their own habitat suitability.

5. Conclusions

600   The aim of this study was to distinguish physical from biological mixing over timescales, using tracers that target
       different grain size fractions. We did not observe clear layering in sediment composition that would point to
       unbioturbated storm deposits. We showed that sand fractions and mud fractions are mixed differently: fine tracers
       showed clear signs of bioturbation, while the sand fraction appeared to be less intensely bioturbated than we
       expected. In conclusion, mud is more mobile within the sediment matrix, due to its higher likelihood to be mixed
605   by bioturbation and physical processes. Sand grains are overall more static and have a higher potential to conserve
       layering, although single-grain feldspar luminescence signals also showed signs of bioturbation. Over long
       (decadal) timescales and in dynamic or young environments, it remains impossible to distinguish sediment grains
       mixed by storms from those reworked by bioturbation with full certainty. Nevertheless, the combination of
       luminescence signals with different bleaching characteristics can give a more complete picture of the deposition
610   and reworking of sand grains. Multi-grain quartz luminescence was suitable for dating sand grains, while single-
       grain feldspar luminescence gave information on mixing processes. If applied in consideration of the local
       environmental conditions, the single-grain signals are a promising technique for tracing bioturbation, but this
       application needs to be tested further. Until then, a combination of short- and long-term tracers is needed to draw
       robust conclusions on sediment mixing processes at dynamic intertidal sites.

615

Appendix A

A1 Core samples

Table A1. length per core and analysed samples from long cores.

	Sandy site	Muddy site
Length XRF and grain size core (m)	0.74	0.65
Length luminescence and ^{210}Pb core (m)	0.75	0.72
Number of luminescence samples	8	8
Number of ^{210}Pb samples	13	13
Sample intervals for ^{210}Pb and **luminescence** (cm)	**0–2.5**	**0–2.5**
	5–7.5	**5–7.5**
	10–12.5	**10–12.5**
	15–17.5	**15–17.5**
	20–22.5	22.5–25
	32.5–35	27.5–30
	40–42.5	**35–37.5**
	50–52.5	**40–42.5**
	52.5–55	**50–52.5**
	57.5–60	**55–57.5**
	62.5–65	57.5–60
	67.5–70	65–67.5
	72.5–75	70–72.5

A2 Luminescence analysis

A2.1 Equivalent dose measurements

620 The luminescence samples were prepared at the Netherlands Centre for Luminescence Dating (NCL) under amber light conditions. After obtaining the 212–250 μm grain size fraction by wet sieving, carbonates were removed by treating the material with a 10 % HCl solution, followed by the removal of organic matter using a 10 % H_2O_2 solution. Magnetic particles were removed by using a Frantz magnetic separator at a current of 1.4 A on the
625 magnet and under an angle of 10° (Porat, 2006). A K-feldspar-rich fraction was extracted through density separation using a separating funnel and LST Fastfloat© with a density of 2.58 g cm^{-3} and washed with demineralized water. A quartz-rich fraction was subsequently isolated from the heavy fraction by performing an additional density separation with LST of 2.70 g cm^{-3}. The quartz fraction was then rinsed with a 10 % HF solution, followed by treatment with a 40 % HF solution to dissolve feldspar and/or other contaminants and etch the outer
630 skin of quartz grains. Afterward, the material was rinsed with HCl, demineralized water, dried, and sieved.

Each multi-grain quartz sample was measured using an automated Risø TL/OSL DA-15 reader with a calibrated ^{90}Sr/^{90}Y beta source. Blue (~470 nm) light emitting diodes (LEDs) were used for optical stimulation. The quartz OSL signals were detected through a 7.5 mm Hoya U-340 filter with a UV detection window. A Single-Aliquot Regenerative-dose protocol (SAR) (Table 2) was used: 1000 datapoints were read out during 20 s of stimulation
635 at 125 °C (0.020 s per datapoint). Channels 1 up to 25 (0.5 s) were taken as initial integration interval; the

background interval was set at channel 26 up to 88 (1.24 s). A linear fit was used for dose-response curve fitting, and the curve was forced through the origin. Rejection criteria (recycling ratio, recuperation rate, and test dose error) were set at 15 %. The recuperation rate was taken relative to the first regenerative dose point.

640   All single-grain feldspar measurements were conducted using an automated Risø TL/OSL DA-20 reader with an automated detection and stimulation head (DASH) and an EMCCD camera (Kook et al., 2015). The system is equipped with a calibrated $^{90}Sr/^{90}Y$ beta source, delivering a dose rate of approximately 0.0707 Gy/s to the feldspar grains on a single-grain disc. To target the 410 nm peak emission of K-feldspar, a blue filter package, BG-3+BG-39 (3.0 + 4.0 mm) was used. A fading test was not conducted. Using a multiple-elevated-temperature (MET) pIRIR measurement protocol was used (de Boer et al., 2024b; Li and Li, 2011), a total of 270 datapoints were

645   recorded in 108 seconds (0.400 seconds per datapoint), with 250 datapoints collected during stimulation. For each sample, three single-grain discs were measured, which would correspond to 300 grains if all positions were filled. However, visual inspection revealed that some positions were unoccupied, resulting in an estimated total of approximately 250 grains measured per sample. Channels 11 up to 15 (2 s) were taken as initial integration interval; the background interval was set at channel 226 up to 250 (9.6 s). A linear fit was used for dose-response

650   curve fitting, and the curve was forced through the origin. Rejection criteria (recycling ratio, recuperation rate, and test dose error) were set at 20 %. The recuperation rate was taken relative to the fourth regenerative dose point.

A2.2 Dose rate measurements

To prepare samples for gamma spectrometry samples were first dried and ashed, documenting weight loss to

655   determine water and organic content. Then the samples were grinded and mixed with wax to create a puck of fixed geometry and retain Radon. Activity concentrations of 40K and several nuclides from the Uranium and Thorium decay chains are measured using a high-resolution gamma ray spectrometer.

A3 Benthic community

660   **Table A2.** Benthic community composition at sandy and muddy site and biomass (g ash-free dry weight m^{-1}) per taxon. Note that this table does not include *Arenicola marina*, since this species was not present in the benthic core samples

Sample site	Latin name	Total density (individuals m^{-2})	Total biomass (g AFDW m^{-2})
Sandy site	*Capitella capitata*	226	0.12
	Carcinus maenas	56	0.38
	Cirratulida	169	0.16
	Crangon crangon	56	0.37
	Eteone longa	56	0.09
	Lanice conchilega	56	0.77
	Macoma balthica	56	0.18
	Nereididae	56	0.10
	Oligochaeta	395	0.15
	Pygospio elegans	621	0.15
	Scoloplos armiger	508	1.19
	Urothoe poseidonis	226	0.18
	Sum	**2486**	**3.84**
Muddy site	*Amphipoda*	0*	0.14
	Bivalvia	113	0.13
	Capitella capitata	452	0.20
	Cirratulida	960	0.27
	Corophium volutator	56	0.11
	Eteone longa	1017	0.47
	Gammaridae	169	0.12
	Hediste diversicolor	395	5.97
	Heteromastus filiformis	1186	3.66
	Macoma balthica	226	0.55
	Nereididae	1017	0.26
	Oligochaeta	17514	1.47
	Pygospio elegans	3503	0.37
	Scoloplos armiger	169	0.11
	Scrobicularia plana	282	5.13
	Urothoe	113	0.12
	Sum	**27175**	**19.07**

* as the number of individuals is determined by headcount, when only body parts without head are present, the individuals are identified to the lowest taxonomic level and only analysed for biomass.

665
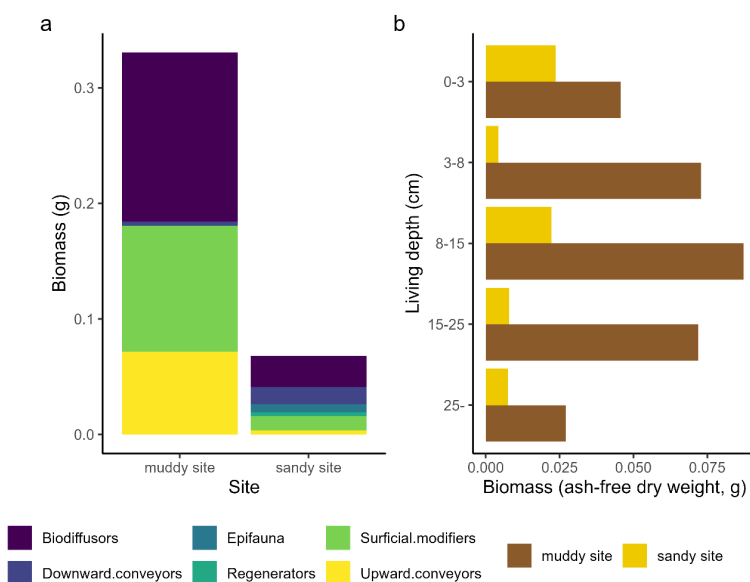
Figure A1: Bioturbation and depth traits from the benthic community, comparing both sites. Relative trait scores for bioturbation mode (a) and living depth (b) are multiplied with total biomass per taxon. Note that this figure does not include *Arenicola marina*, since this species were not present in the benthic core sa

670

A4 Luminescence modelled palaeodose, dose rate and modelled age

Table A3a. Multi-grain quartz luminescence results.

NCL-code	Depth [m]	MG-QZ Palaeodose [Gy]			QZ Dose rate [Gy/ka]	MG-QZ Age [a]		
		Iterated	CAM	bootMAM		Iterated	CAM	bootMAM
Sandy core								
NCL-2423121	**0.015**	0.04 ± 0.01	0.05 ± 0.01	0.01 ± 0	1.22 ± 0.06	36.1 ± 6.3	43 ± 12.0	9.4 ± 2.8
NCL-2423123	**0.05**	0.05 ± 0.01	0.09 ± 0.02	0.03 ± 0.01	1.3 ± 0.06	41.6 ± 6.2	67.6 ± 16.8	20.4 ± 8.5
NCL-2423125	**0.1**	0.04 ± 0.01	0.09 ± 0.02	0.1 ± 0.03	1.32 ± 0.05	32.2 ± 6.7	70.4 ± 14.2	73.2 ± 19.9
NCL-2423127	**0.15**	0.02 ± 0.01	0.09 ± 0.02	0.06 ± 0.04	1.27 ± 0.06	19.6 ± 4.7	73.1 ± 18	49.3 ± 31.7
NCL-2423129	**0.2**	0.1 ± 0.02	0.13 ± 0.03	0.1 ± 0.04	1.34 ± 0.06	74.1 ± 13.9	95.6 ± 19.7	78.1 ± 26.5
NCL-2423134	**0.33**	0.06 ± 0.01	0.09 ± 0.01	0.09 ± 0.02	1.23 ± 0.05	48.8 ± 8.6	69.8 ± 8.1	74.5 ± 16.6
NCL-2423137	**0.4**	0.08 ± 0.01	0.09 ± 0.02	0.05 ± 0	1.08 ± 0.04	72.5 ± 9.4	84 ± 14.8	45.1 ± 2
NCL-2423141	**0.5**	0.6 ± 0.04	0.63 ± 0.06	0.49 ± 0.01	1.41 ± 0.06	428.3 ± 37	449.5 ± 46.3	345 ± 17.2
Muddy core								
NCL-2323092	**0.015**	0.04 ± 0.01	0.07 ± 0.02	0.04 ± 0.02	1.28 ± 0.07	27.5 ± 5.4	55.6 ± 13.7	27.5 ± 14.7
NCL-2323094	**0.05**	0.03 ± 0.01	0.07 ± 0.02	0.03 ± 0.02	1.31 ± 0.06	22.3 ± 4.8	49.6 ± 13.4	21.2 ± 12.6
NCL-2323096	**0.1**	0.04 ± 0.01	0.07 ± 0.02	0.01 ± 0.01	1.33 ± 0.06	31.3 ± 5.9	54.4 ± 17.5	10.8 ± 6.3
NCL-2323098	**0.15**	0.04 ± 0.01	0.1 ± 0.03	0.02 ± 0.01	1.24 ± 0.06	33.8 ± 7.9	79 ± 27.9	17.9 ± 11.5
NCL-2323106	**0.35**	0.56 ± 0.02	0.57 ± 0.03	0.57 ± 0.06	1.23 ± 0.06	455.1 ± 29.1	459.6 ± 30	458.3 ± 51.9
NCL-2323108	**0.4**	0.63 ± 0.04	0.63 ± 0.03	0.61 ± 0.06	1.42 ± 0.07	442.2 ± 33	445 ± 29.7	432.3 ± 49.8
NCL-2323112	**0.5**	0.81 ± 0.07	0.87 ± 0.1	0.55 ± 0.1	1.59 ± 0.08	508.5 ± 50.7	546.6 ± 66.9	346.9 ± 66.9
NCL-2323114	**0.55**	0.91 ± 0.03	0.99 ± 0.05	0.96 ± 0.09	1.55 ± 0.08	585.3 ± 34.7	635.1 ± 43.5	619.8 ± 66

675 **Table A3b.** Single-grain IRSL50 luminescence results.

NCL-code	Depth [m]	SG-FS IRSL50 Palaeodose [Gy]			FS Dose rate [Gy/ka]	SG-FS IRSL50 Age [a]		
		Iterated	CAM	bootMAM		Iterated	CAM	bootMAM
Sandy core								
NCL-2423121	0.015	0.15 ± 0.03	0.26 ± 0.07	0.16 ± 0	2.1 ± 0.08	72.4 ± 16.7	125.8 ± 32.1	75.9 ± 3.3
NCL-2423123	0.05	0.24 ± 0.05	0.33 ± 0.07	0.12 ± 0.03	2.19 ± 0.08	108.9 ± 21.1	152.6 ± 31.3	53.3 ± 15.6
NCL-2423125	0.1	0.21 ± 0.02	0.22 ± 0.02	0.22 ± 0.04	2.21 ± 0.08	93.0 ± 10.5	99.2 ± 9.5	101.5 ± 19.1
NCL-2423127	0.15	0.09 ± 0.02	0.15 ± 0.04	0.15 ± 0.06	2.16 ± 0.08	42.2 ± 7.4	70.4 ± 20.5	69.2 ± 28.1
NCL-2423129	0.2	0.18 ± 0.03	0.25 ± 0.05	0.08 ± 0.02	2.23 ± 0.08	79.3 ± 12	113.1 ± 22.5	33.8 ± 11.0
NCL-2423134	0.33	0.09 ± 0.01	0.14 ± 0.02	0.09 ± 0	2.12 ± 0.07	43.6 ± 5.2	66.3 ± 9.2	40.5 ± 1.6
NCL-2423137	0.4	0.25 ± 0.04	0.27 ± 0.03	0.27 ± 0.05	1.96 ± 0.07	126.5 ± 18.5	137 ± 15.2	136.1 ± 26.8
NCL-2423141	0.5	0.66 ± 0.05	0.71 ± 0.05	0.58 ± 0.1	2.29 ± 0.08	289 ± 24.7	310.6 ± 26.2	253.9 ± 43.2
Muddy core								
NCL-2323092	0.015	0.1 ± 0.01	0.2 ± 0.04	0.1 ± 0.02	2.17 ± 0.09	45.5 ± 6.0	90.7 ± 17.0	44.4 ± 11.5
NCL-2323094	0.05	0.14 ± 0.01	0.22 ± 0.03	0.1 ± 0.03	2.2 ± 0.08	64.5 ± 7.2	100.3 ± 16.0	44.4 ± 13.2
NCL-2323096	0.1	0.18 ± 0.02	0.27 ± 0.04	0.11 ± 0.04	2.21 ± 0.08	83.6 ± 9.5	123.0 ± 20.7	50.9 ± 16.4
NCL-2323098	0.15	0.16 ± 0.02	0.29 ± 0.05	0.18 ± 0.05	2.12 ± 0.08	75 ± 9.0	134.2 ± 22.1	86.2 ± 24.0
NCL-2323106	0.35	0.78 ± 0.04	0.83 ± 0.07	0.78 ± 0.1	2.12 ± 0.08	370.0 ± 24.7	392.9 ± 35.1	369.6 ± 48.4
NCL-2323108	0.4	0.74 ± 0.08	0.82 ± 0.07	0.72 ± 0.13	2.31 ± 0.09	322.6 ± 38.8	356.7 ± 34.5	311.9 ± 55.8
NCL-2323112	0.5	0.69 ± 0.07	0.76 ± 0.07	0.72 ± 0.01	2.48 ± 0.1	276.1 ± 31.4	305.4 ± 31.2	291.8 ± 12.8
NCL-2323114	0.55	0.9 ± 0.09	0.97 ± 0.08	0.95 ± 0.02	2.44 ± 0.09	369.6 ± 40.7	396.0 ± 34.9	390.9 ± 17

Table A3c. Single-grain pIR175 luminescence results.

NCL-code	Depth [m]	SG-FS pIR175 Palaeodose [Gy]			FS Dose rate [Gy/ka]	SG-FS pIR175 Age [a]		
		Iterated	**CAM**	**bootMAM**		**Iterated**	**CAM**	**bootMAM**
Sandy core								
NCL-2423121	**0.015**	0.37 ± 0.1	0.47 ± 0.13	0.2 ± 0.08	2.1 ± 0.08	177.1 ± 47.5	222.6 ± 61.9	94.4 ± 39.4
NCL-2423123	**0.05**	0.35 ± 0.04	0.45 ± 0.07	0.25 ± 0.08	2.19 ± 0.08	157.8 ± 21.0	205.9 ± 34.0	113.2 ± 36.2
NCL-2423125	**0.1**	0.43 ± 0.06	0.45 ± 0.07	0.37 ± 0.12	2.21 ± 0.08	193.2 ± 30.1	206.1 ± 32.9	166.5 ± 53.3
NCL-2423127	**0.15**	0.2 ± 0.04	0.38 ± 0.07	0.32 ± 0.1	2.16 ± 0.08	92.9 ± 16.98	176.3 ± 32.1	149.8 ± 46.5
NCL-2423129	**0.2**	0.33 ± 0.04	0.32 ± 0.05	0.17 ± 0.04	2.23 ± 0.08	149.0 ± 20.02	145.9 ± 21.3	74.9 ± 17.7
NCL-2423134	**0.33**	0.24 ± 0.02	0.3 ± 0.03	0.2 ± 0	2.12 ± 0.07	115.6 ± 8.22	140.6 ± 14.1	93.8 ± 3.8
NCL-2423137	**0.4**	0.46 ± 0.04	0.49 ± 0.07	0.26 ± 0.07	1.96 ± 0.07	234.1 ± 22.61	249.9 ± 35.0	131.0 ± 36.5
NCL-2423141	**0.5**	1.08 ± 0.08	1.01 ± 0.08	0.89 ± 0.14	2.29 ± 0.08	471.6 ± 37.92	442.4 ± 36.8	387.5 ± 60.9
Muddy core								
NCL-2323092	**0.013**	0.3 ± 0.04	0.42 ± 0.07	0.18 ± 0.04	2.17 ± 0.09	138.0 ± 20.6	191.4 ± 32.7	81.8 ± 19.2
NCL-2323094	**0.05**	0.37 ± 0.06	0.52 ± 0.09	0.2 ± 0.06	2.2 ± 0.08	166.5 ± 29.9	235.1 ± 43.9	90.9 ± 25.6
NCL-2323096	**0.1**	0.26 ± 0.03	0.39 ± 0.07	0.19 ± 0.05	2.21 ± 0.08	116.0 ± 14.9	174.3 ± 30.2	86.7 ± 20.9
NCL-2323098	**0.15**	0.4 ± 0.06	0.37 ± 0.07	0.16 ± 0.04	2.12 ± 0.08	186.4 ± 28.6	176.5 ± 33.2	73.1 ± 17.7
NCL-2323106	**0.35**	1.44 ± 0.16	1.49 ± 0.15	0.99 ± 0.19	2.12 ± 0.08	681.2 ± 78.9	705.5 ± 75.3	466.3 ± 91.6
NCL-2323108	**0.4**	1.29 ± 0.06	1.29 ± 0.09	1.22 ± 0.17	2.31 ± 0.09	558 ± 34.9	558.3 ± 46.4	529.4 ± 75.6
NCL-2323112	**0.5**	1.12 ± 0.1	1.08 ± 0.1	1.09 ± 0.18	2.48 ± 0.1	452.6 ± 45.5	436.7 ± 44.8	437.3 ± 72.8
NCL-2323114	**0.55**	1.27 ± 0.14	1.35 ± 0.13	1.17 ± 0.23	2.44 ± 0.09	519.7 ± 59.1	553.5 ± 57.8	478.9 ± 96.3

680

A5 Luminophore observations
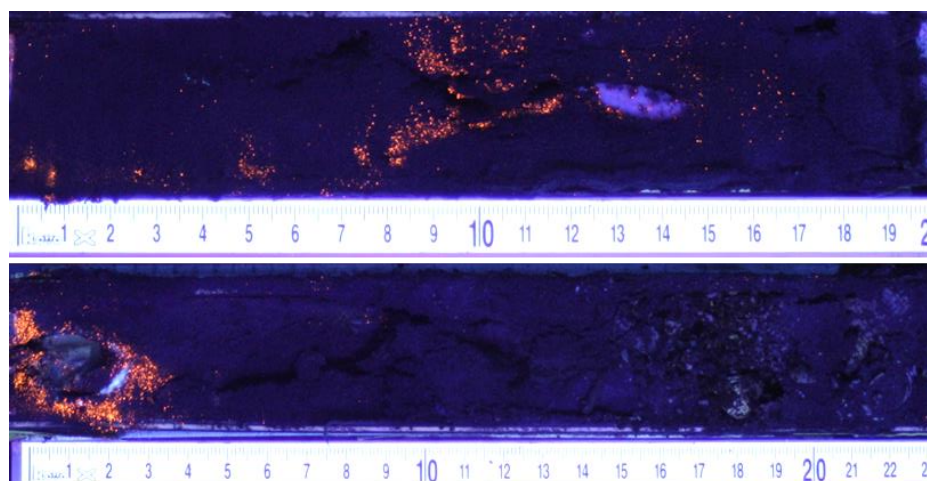
Figure A2: Cores taken 36 hours after luminophore application, indicating observations of downward particle transport reworking by *S. plana* at sandy site (top) and *C. edule* at muddy site (bottom).

685
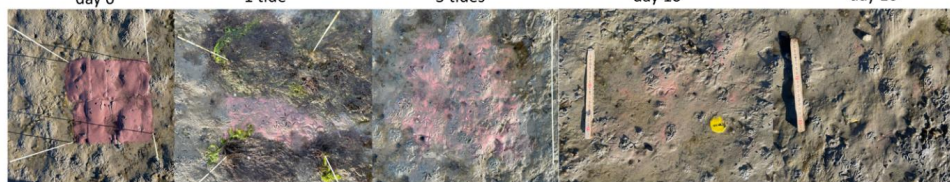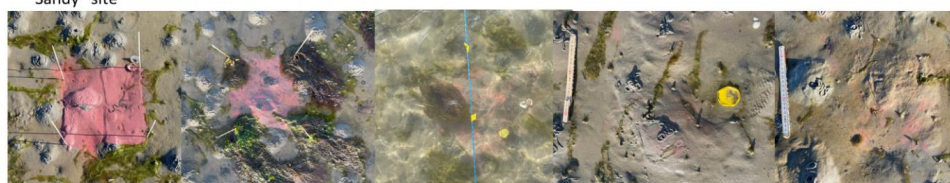
Figure A3: Observations of luminophores on the sediment surface. Note the decrease in luminophores visible on the surface. The sticks placed at the start of the experiment were removed after 1 tide, as they were observed to trap algae.

690

Code and data availability

Data and code used for the analysis in this study will be made openly available upon publication. During the review process, reviewer assets can be accessed through www.doi.org/10.25850/nioz/7b.b.ak, using the credentials provided to the reviewers.

695 **Author contribution**

Tjitske J. Kooistra: Conceptualization, Writing – review & editing, Writing – original draft, Visualization, Software, Project administration, Methodology, Formal analysis, Investigation, Data curation.

Anna-Maartje de Boer: Conceptualization, Writing – review & editing, Writing – original draft, Visualization, Software, Methodology, Formal analysis, Investigation, Data curation.

700 **Tjeerd J. Bouma**: Conceptualization, Writing – review & editing, Supervision.

Natascia Pannozzo: Conceptualization, Writing – review & editing, Investigation.

Stuart G. Pearson: Conceptualization, Writing – review & editing, Supervision, Funding acquisition.

Ad van der Spek: Conceptualization, Writing – review & editing, Funding acquisition.

Henko de Stigter: Conceptualization, Writing – review & editing, Resources.

705 **Jakob Wallinga:** Conceptualization, Writing – review & editing, Investigation, Resources, Funding acquisition.

Rob Witbaard: Conceptualization, Writing – review & editing, Supervision, Project administration, Funding acquisition, Conceptualization.

Karline Soetaert: Conceptualization, Writing – review & editing, Supervision.

Competing interests

710 The authors declare that they have no conflict of interest.

Acknowledgements

We would like to thank Erna van de Hengel-Voskuilen, Bartel Komin, Birte Leutelt, Bram Parmentier, Eva Lansu, Carlijn Lammers, Paula de la Barra and Sarah Manni for help with field sampling; Erna van de Hengel-Voskuilen and Alice Versendaal for help with luminescence laboratory analysis and preparation of data; Piet van Gaever and

715 Jeroen Kooijman for XRF and ^{210}Pb analysis and preparation of data; Peter van Breugel for grain size analysis; Jurian Brasser for assistance with Chl-*a* analysis; and Lennart van IJzerloo and Birte Leutelt for help with luminophore analysis. Funding for this study was provided by NWO grant no. 17600: "Tracking Ameland Inlet Living Lab Sediment (TRAILS)". Additionally, Stuart Pearson received funding from NWO grant no. 21026: "Revealing Hidden Networks of Coastal Sediment Pathways".

720 **Financial support**

- NWO grant no. 17600: "Tracking Ameland Inlet Living Lab Sediment (TRAILS)"
- NWO grant no. 21026: "Revealing Hidden Networks of Coastal Sediment Pathways"

References

Aller, R. C.: The Effects of Macrobenthos on Chemical Properties of Marine Sediment and Overlying Water, in:

725 Animal-sediment relations: the biogenic alteration of sediments., vol. 100, edited by: McCall, P. L. and Tevesz, M. J. S., Springer Science & Business Media, Boston, MA, 53–102, https://doi.org/10.1007/978-1-4757-1317-6_2, 1982.

Aller, R. C. and Cochran, J. K.: The Critical Role of Bioturbation for Particle Dynamics, Priming Potential, and Organic C Remineralization in Marine Sediments: Local and Basin Scales, Front Earth Sci (Lausanne), 7, 459885,
730   https://doi.org/10.3389/feart.2019.00157, 2019.

Armanini, A.: Non-uniform sediment transport: dynamics of the active layer, Journal of Hydraulic Research, 33, 611–622, https://doi.org/10.1080/00221689509498560, 1995.

Baumfalk, Y. A.: Heterogeneous grain size distribution in tidal flat sediment caused by bioturbation activity of Arenicola marina (polychaeta), Netherlands Journal of Sea Research, 13, 428–440, https://doi.org/10.1016/0077-
735   7579(79)90016-4, 1979.

Beauchard, O., Bradshaw, C., Bolam, S., Tiano, J., Garcia, C., De Borger, E., Laffargue, P., Blomqvist, M., Tsikopoulou, I., Papadopoulou, N. K., Smith, C. J., Claes, J., Soetaert, K., and Sciberras, M.: Trawling-induced change in benthic effect trait composition – A multiple case study, Front Mar Sci, 10, 1303909, https://doi.org/10.3389/fmars.2023.1303909, 2023.

740   Belliard, J. P., Silinski, A., Meire, D., Kolokythas, G., Levy, Y., Van Braeckel, A., Bouma, T. J., and Temmerman, S.: High-resolution bed level changes in relation to tidal and wave forcing on a narrow fringing macrotidal flat: Bridging intra-tidal, daily and seasonal sediment dynamics, Mar Geol, 412, 123–138, https://doi.org/10.1016/j.margeo.2019.03.001, 2019.

Benninger, L. K., Aller, R. C., Cochran, J. K., and Turekian, K. K.: Effects of biological sediment mixing on the
745   210Pb chronology and trace metal distribution in a Long Island Sound sediment core, Earth Planet Sci Lett, 43, 241–259, https://doi.org/10.1016/0012-821X(79)90208-5, 1979.

Bentley, S. J. and Nittrouer, C. A.: Accumulation and intense bioturbation of bioclastic muds along a carbonate-platform margin: Dry Tortugas, Florida, Mar Geol, 315–318, 44–57, https://doi.org/10.1016/j.margeo.2012.05.002, 2012.

750   Bentley, S. J., Swales, A., Pyenson, B., and Dawe, J.: Sedimentation, bioturbation, and sedimentary fabric evolution on a modern mesotidal mudflat: A multi-tracer study of processes, rates, and scales, Estuar Coast Shelf Sci, 141, 58–68, https://doi.org/10.1016/j.ecss.2014.02.004, 2014.

de Boer, A. M., Seebregts, M., Wallinga, J., and Chamberlain, E.: A one-day experiment quantifying subaqueous bleaching of K-feldspar luminescence signals in the Wadden Sea, the Netherlands, Netherlands Journal of
755   Geosciences, 103, e22, https://doi.org/10.1017/njg.2024.18, 2024a.

de Boer, A. M., Kook, M., and Wallinga, J.: Testing the performance of an EMCCD camera in measuring single-grain feldspar (thermo)luminescence in comparison to a laser-based single-grain system, Radiat Meas, 175, 107168, https://doi.org/10.1016/j.radmeas.2024.107168, 2024b.

de Boer, A. M., Pannozzo, N., Pearson, S. G., Kooistra, T. J., van Prooijen, B. C., and Wallinga, J.: Subaqueous
760   resetting of the luminescence clock: bleaching of sand-sized quartz and feldspar in coastal waters, n.d.

Bolam, S. G. and Fernandes, T. F.: Dense aggregations of Pygospio elegans (Claparède): Effect on macrofaunal community structure and sediments, J Sea Res, 49, 171–185, https://doi.org/10.1016/S1385-1101(03)00007-8, 2003.

Brückner, M. Z. M., Schwarz, C., Coco, G., Baar, A., Boechat Albernaz, M., and Kleinhans, M. G.: Benthic
765   species as mud patrol - modelled effects of bioturbators and biofilms on large-scale estuarine mud and morphology, Earth Surf Process Landf, 46, 1128–1144, https://doi.org/10.1002/esp.5080, 2021.

Cadee, G. C.: Sediment reworking by Arenicola marina on tidal flats in the Dutch Wadden Sea, Netherlands Journal of Sea Research, 10, 440–460, 1976.

Carey, D. A.: Sedimentological effects and palaeoecological implications of the tube-building polychaete Lanice

770 conchilega Pallas, Sedimentology, 34, 49–66, https://doi.org/10.1111/j.1365-3091.1987.tb00559.x, 1987.

Choi, J., Van Beek, R., Chamberlain, E. L., Reimann, T., Smeenge, H., Van Oorschot, A., and Wallinga, J.: Luminescence dating approaches to reconstruct the formation of plaggic anthrosols, SOIL, 10, 567–586, https://doi.org/10.5194/soil-10-567-2024, 2024.

Colarossi, D., Duller, G. A. T., Roberts, H. M., Tooth, S., and Lyons, R.: Comparison of paired quartz OSL and

775 feldspar post-IR IRSL dose distributions in poorly bleached fluvial sediments from South Africa, Quat Geochronol, 30, 233–238, https://doi.org/10.1016/j.quageo.2015.02.015, 2015.

Colosimo, I., van Maren, D. S., de Vet, P. L. M., Winterwerp, J. C., and van Prooijen, B. C.: Winds of opportunity: The effects of wind on intertidal flat accretion, Geomorphology, 439, 108840, https://doi.org/10.1016/j.geomorph.2023.108840, 2023.

780 Compton, T. J., Holthuijsen, S., Koolhaas, A., Dekinga, A., Smith, J., Galama, Y., Brugge, M., Wal, D. Van Der, and Meer, J. Van Der: Distinctly variable mudscapes: Distribution gradients of intertidal macrofauna across the Dutch Wadden Sea, J Sea Res, 82, 103–116, https://doi.org/10.1016/j.seares.2013.02.002, 2013.

Croudace, I. W., Rindby, A., and Rothwell, R. G.: ITRAX: Description and evaluation of a new multi-function X-ray core scanner, Geol Soc Spec Publ, 267, 51–63, https://doi.org/10.1144/GSL.SP.2006.267.01.04, 2006.

785 Cunningham, A. C. and Wallinga, J.: Realizing the potential of fluvial archives using robust OSL chronologies, Quat Geochronol, 12, 98–106, https://doi.org/10.1016/j.quageo.2012.05.007, 2012.

Cunningham, A. C., Buylaert, J. P., and Murray, A. S.: Attenuation of beta radiation in granular matrices: implications for trapped-charge dating, Geochronology, 4, 517–531, https://doi.org/10.5194/gchron-4-517-2022, 2022.

790 Davison, C.: IV.—On the amount of sand brought up by Lobworms to the surface, Geol Mag, 8, 489–493, https://doi.org/10.1017/S0016756800187497, 1891.

Deloffre, J., Verney, R., Lafite, R., Lesueur, P., Lesourd, S., and Cundy, A. B.: Sedimentation on intertidal mudflats in the lower part of macrotidal estuaries: Sedimentation rhythms and their preservation, Mar Geol, 241, 19–32, https://doi.org/10.1016/j.margeo.2007.02.011, 2007.

795 Fan, D., Guo, Y., Wang, P., and Shi, J. Z.: Cross-shore variations in morphodynamic processes of an open-coast mudflat in the Changjiang Delta, China: With an emphasis on storm impacts, Cont Shelf Res, 26, 517–538, https://doi.org/10.1016/j.csr.2005.12.011, 2006.

Foster-Smith, R. L.: An analysis of water flow in tube-living animals, J Exp Mar Biol Ecol, 34, 73–95, https://doi.org/10.1016/0022-0981(78)90058-8, 1978.

800 François, F., Poggiale, J. C., Durbec, J. P., and Stora, G.: A new approach for the modelling of sediment reworking induced by a macrobenthic community, Acta Biotheor, 45, 295–319, https://doi.org/10.1023/a:1000636109604, 1997.

Frithsen, J. B. and Doering, P. H.: Active enhancement of particle removal from the water column by tentaculate benthic polychaetes, Ophelia, 25, 169–182, https://doi.org/10.1080/00785326.1986.10429748, 1986.

805   Galbraith, R. F., Roberts, R. G., Laslett, G. M., Yoshida, H., and Olley, J. M.: Optical dating of single and multiple grains of quartz form Jinmium Rock Shelter, Northern Australia: Part I, experimental design and statistical models, Archaeometry, 41, 339–364, https://doi.org/10.1111/j.1475-4754.1999.tb00987.x, 1999.

Gao, S.: Geomorphology and sedimentology of tidal flats, in: Coastal Wetlands: An Integrated Ecosystem Approach, Elsevier, 359–381, https://doi.org/10.1016/B978-0-444-63893-9.00010-1, 2018.

810   Gebhardt, C. and Forster, S.: Size-selective feeding of Arenicola marina promotes long-term burial of microplastic particles in marine sediments, Environmental Pollution, 242, 1777–1786, https://doi.org/10.1016/j.envpol.2018.07.090, 2018.

Gerino, M., Aller, R. C., Lee, C., Cochran, J. K., Aller, J. Y., Green, M. A., and Hirschberg, D.: Comparison of different tracers and methods used to quantify bioturbation during a spring bloom: 234-thorium, luminophores
815   and chlorophyll a, Estuar Coast Shelf Sci, 46, 531–547, https://doi.org/10.1006/ecss.1997.0298, 1998.

Godfrey-Smith, D. I., Huntley, D. J., and Chen, W. H.: Optical dating studies of quartz and feldspar sediment extracts, Quat Sci Rev, 7, 373–380, https://doi.org/10.1016/0277-3791(88)90032-7, 1988.

Grandjean, T. J., de Smit, J. C., van Belzen, J., Fivash, G. S., van Dalen, J., Ysebaert, T., and Bouma, T. J.: Morphodynamic signatures derived from daily surface elevation dynamics can explain the morphodynamic
820   development of tidal flats, Water Science and Engineering, 16, 14–25, https://doi.org/10.1016/j.wse.2022.11.003, 2023.

Gray, J. S.: Animal-sediment relationships., Oceanogr. Mar. Biol. Ann. Rev., 12, 223–261, 1974.

Guyard, H., Chapron, E., St-Onge, G., Anselmetti, F. S., Arnaud, F., Magand, O., Francus, P., and Mélières, M. A.: High-altitude varve records of abrupt environmental changes and mining activity over the last 4000 years in
825   the Western French Alps (Lake Bramant, Grandes Rousses Massif), Quat Sci Rev, 26, 2644–2660, https://doi.org/10.1016/j.quascirev.2007.07.007, 2007.

Guyez, A., Bonnet, S., Reimann, T., Carretier, S., and Wallinga, J.: A Novel Approach to Quantify Sediment Transfer and Storage in Rivers—Testing Feldspar Single-Grain pIRIR Analysis and Numerical Simulations, J Geophys Res Earth Surf, 128, e2022JF006727, https://doi.org/10.1029/2022JF006727, 2023.

830   Heimsath, A. M., Chappell, J., Spooner, N. A., and Questiaux, D. G.: Creeping soil, Geology, 30, 111–114, https://doi.org/10.1130/0091-7613(2002)030<0111:CS>2.0.CO;2, 2002.

Herringshaw, L. G., Sherwood, O. A., and McIlroy, D.: Ecosystem engineering by bioturbating polychaetes in event bed microcosms, Palaios, 25, 46–58, https://doi.org/10.2110/palo.2009.p09-055r, 2010.

Le Hir, P., Monbet, Y., and Orvain, F.: Sediment erodability in sediment transport modelling: Can we account for
835   biota effects?, Cont Shelf Res, 27, 1116–1142, https://doi.org/10.1016/j.csr.2005.11.016, 2007.

Hu, Z., van der Wal, D., Cai, H., van Belzen, J., and Bouma, T. J.: Dynamic equilibrium behaviour observed on two contrasting tidal flats from daily monitoring of bed-level changes, Geomorphology, 311, 114–126, https://doi.org/10.1016/j.geomorph.2018.03.025, 2018.

Huettel, M., Berg, P., and Kostka, J. E.: Benthic exchange and biogeochemical cycling in permeable sediments,
840   Ann Rev Mar Sci, 6, 23–51, https://doi.org/10.1146/annurev-marine-051413-012706, 2014.

Jumars, P. A. and Nowell, A. R. M.: Effects of benthos on sediment transport: difficulties with functional grouping, Cont Shelf Res, 3, 115–130, https://doi.org/10.1016/0278-4343(84)90002-5, 1984.

Jumars, P. A., Self, R. F. l., and Nowell, A. R. M.: Mechanics of particle selection by tentaculate deposit-feeders, J Exp Mar Biol Ecol, 64, 47–70, https://doi.org/10.1016/0022-0981(82)90067-3, 1982.

845   Jumars, P. A., Dorgan, K. M., and Lindsay, S. M.: Diet of worms emended: An update of polychaete feeding guilds, Ann Rev Mar Sci, 7, 497–520, https://doi.org/10.1146/annurev-marine-010814-020007, 2015.

Kars, R. H., Busschers, F. S., and Wallinga, J.: Validating post IR-IRSL dating on K-feldspars through comparison with quartz OSL ages, Quat Geochronol, 12, 74–86, https://doi.org/10.1016/j.quageo.2012.05.001, 2012.

Kooistra, T. J., Witbaard, R., Bouma, T. J., Pearson, S. G., Bijleveld, A. I., van der Heide, T., Franken, O., and

850   Soetaert, K.: Coarsening coasts: quantifying sensitivity of benthic communities to sandification, Estuar Coast Shelf Sci, 320, 109303, https://doi.org/10.1016/j.ecss.2025.109303, 2025.

Kook, M., Lapp, T., Murray, A. S., Thomsen, K. J., and Jain, M.: A luminescence imaging system for the routine measurement of single-grain OSL dose distributions, Radiat Meas, 81, 171–177, https://doi.org/10.1016/j.radmeas.2015.02.010, 2015.

855   Kreutzer, S., Burow, C., Dietze, M., Fuchs, M. C., Schmidt, C., Fischer, M., Friedrich, J., Mercier, N., Smedley, R., Christophe, C., Zink, A., Durcan, J. A., King, G. E., Philippe, A., Guérin, G., Riedesel, S., Autzen, M., Guibert, P., Mittelstraß, D., Gray, H. J., Galharret, J. M., and Fuchs, M.: Luminescence 1.X: Comprehensive Luminescence Dating Data Analysis, https://doi.org/10.5281/ZENODO.596252, 2025.

Kristensen, E., Penha-Lopes, G., Delefosse, M., Valdemarsen, T., Quintana, C. O., and Banta, G. T.: What is

860   bioturbation? the need for a precise definition for fauna in aquatic sciences, Mar Ecol Prog Ser, 446, 285–302, https://doi.org/10.3354/meps09506, 2012.

Kristensen, J. A., Thomsen, K. J., Murray, A. S., Buylaert, J. P., Jain, M., and Breuning-Madsen, H.: Quantification of termite bioturbation in a savannah ecosystem: Application of OSL dating, Quat Geochronol, 30, 334–341, https://doi.org/10.1016/j.quageo.2015.02.026, 2015.

865   Lecroart, P., Maire, O., Schmidt, S., Grémare, A., Anschutz, P., and Meysman, F. J. R.: Bioturbation, short-lived radioisotopes, and the tracer-dependence of biodiffusion coefficients, Geochim Cosmochim Acta, 74, 6049–6063, https://doi.org/10.1016/j.gca.2010.06.010, 2010.

Li, B. and Li, S. H.: Luminescence dating of K-feldspar from sediments: A protocol without anomalous fading correction, Quat Geochronol, 6, 468–479, https://doi.org/10.1016/j.quageo.2011.05.001, 2011.

870   Longbottom, M. R.: The distribution of Arenicola marina (L.) with particular reference to the effects of particle size and organic matter of the sediments, J Exp Mar Biol Ecol, 5, 138–157, https://doi.org/10.1016/0022-0981(70)90013-4, 1970.

Madsen, A. T., Murray, A. S., Andersen, T. J., Pejrup, M., and Breuning-Madsen, H.: Optically stimulated luminescence dating of young estuarine sediments: A comparison with 210Pb and 137Cs dating, Mar Geol, 214,

875   251–268, https://doi.org/10.1016/j.margeo.2004.10.034, 2005.

Madsen, A. T., Murray, A. S., Andersen, T. J., and Pejrup, M.: Temporal changes of accretion rates on an estuarine salt marsh during the late Holocene - Reflection of local sea level changes? The Wadden Sea, Denmark, Mar Geol, 242, 221–233, https://doi.org/10.1016/j.margeo.2007.03.001, 2007.

Madsen, A. T., Murray, A. S., Jain, M., Andersen, T. J., and Pejrup, M.: A new method for measuring bioturbation

880   rates in sandy tidal flat sediments based on luminescence dating, Estuar Coast Shelf Sci, 92, 464–471, https://doi.org/10.1016/j.ecss.2011.02.004, 2011.

Maire, O., Lecroart, P., Meysman, F. J. R., Rosenberg, R., Duchêne, J. C., and Grémare, A.: Quantification of sediment reworking rates in bioturbation research: A review, Aquat Biol, 2, 219–238, https://doi.org/10.3354/ab00053, 2008.

885   Mauz, B. and Bungenstock, F.: How to reconstruct trends of late Holocene relative sea level: A new approach using tidal flat clastic sediments and optical dating, Mar Geol, 237, 225–237, https://doi.org/10.1016/j.margeo.2006.12.001, 2007.

Mauz, B., Baeteman, C., Bungenstock, F., and Plater, A. J.: Optical dating of tidal sediments: Potentials and limits inferred from the North Sea coast, Quat Geochronol, 5, 667–678, https://doi.org/10.1016/j.quageo.2010.05.004,
890   2010.

van der Meij, W. M., Riedesel, S., and Reimann, T.: Mixed Signals: interpreting mixing patterns of different soil bioturbation processes through luminescence and numerical modelling, SOIL, 11, 51–66, https://doi.org/10.5194/soil-11-51-2025, 2025.

Meysman, F. J. R., Boudreau, B., and Middelburg, J.: Relations between local, nonlocal, discrete and continuous
895   models of bioturbation, J Mar Res, 61, 2003.

Meysman, F. J. R., Middelburg, J. J., and Heip, C. H. R.: Bioturbation: a fresh look at Darwin's last idea, Trends Ecol Evol, 21, 688–695, https://doi.org/10.1016/j.tree.2006.08.002, 2006.

Meysman, F. J. R., Malyuga, V. S., Boudreau, B. P., and Middelburg, J. J.: A generalized stochastic approach to particle dispersal in soils and sediments, Geochim Cosmochim Acta, 72, 3460–3478,
900   https://doi.org/10.1016/j.gca.2008.04.023, 2008.

Meysman, F. J. R., Boudreau, B., and Middelburg, J.: When and why does bioturbation lead to diffusive mixing?, J Mar Res, 68, 2010.

Montserrat, F., Van Colen, C., Provoost, P., Milla, M., Ponti, M., Van den Meersche, K., Ysebaert, T., and Herman, P. M. J.: Sediment segregation by biodiffusing bivalves, Estuar Coast Shelf Sci, 83, 379–391,
905   https://doi.org/10.1016/j.ecss.2009.04.010, 2009.

Montserrat, F., Suykerbuyk, W., Al-Busaidi, R., Bouma, T. J., van der Wal, D., and Herman, P. M. J.: Effects of mud sedimentation on lugworm ecosystem engineering, J Sea Res, 65, 170–181, https://doi.org/10.1016/j.seares.2010.09.003, 2011.

Morys, C., Powilleit, M., and Forster, S.: Bioturbation in relation to the depth distribution of macrozoobenthos in
910   the southwestern Baltic Sea, Mar Ecol Prog Ser, 579, 19–36, https://doi.org/10.3354/meps12236, 2017.

Ouellette, D., Desrosiers, G., Gagne, J., Gilbert, F., Poggiale, J., Blier, P., and Stora, G.: Effects of temperature on in vitro sediment reworking processes by a gallery biodiffusor, the polychaete Neanthes virens, Mar Ecol Prog Ser, 266, 185–193, https://doi.org/10.3354/meps266185, 2004.

Pannozzo, N., Smedley, R. K., Plater, A. J., Carnacina, I., and Leonardi, N.: Novel luminescence diagnosis of
915   storm deposition across intertidal environments, Science of the Total Environment, 867, 161461, https://doi.org/10.1016/j.scitotenv.2023.161461, 2023.

Porat: Use of magnetic separation for purifying quartz for luminescence dating, Ancient TL, 24, 33–36, 2006.

Prescott, J. R., Fox, P. J., Robertson, G. B., and Hutton, J. T.: Three-dimensional spectral studies of the bleaching of the thermoluminescence of feldspars, Radiat Meas, 23, 367–375, https://doi.org/10.1016/1350-4487(94)90066-
920   3, 1994.

Queirós, A. M., Birchenough, S. N. R., Bremner, J., Godbold, J. A., Parker, R. E., Romero-Ramirez, A., Reiss, H., Solan, M., Somerfield, P. J., Van Colen, C., Van Hoey, G., and Widdicombe, S.: A bioturbation classification of European marine infaunal invertebrates, Ecol Evol, 3, 3958–3985, https://doi.org/10.1002/ECE3.769, 2013.

R Core Team: R: A Language and Environment for Statistical Computing, 2024.

925 Reimann, T., Román-Sánchez, A., Vanwalleghem, T., and Wallinga, J.: Getting a grip on soil reworking – Single-grain feldspar luminescence as a novel tool to quantify soil reworking rates, Quat Geochronol, 42, 1–14, https://doi.org/10.1016/j.quageo.2017.07.002, 2017.

Reise, K.: Sediment mediated species interactions in coastal waters, J Sea Res, 48, 127–141, https://doi.org/10.1016/S1385-1101(02)00150-8, 2002.

930 Rhoads, D. C. and Boyer, L. F.: The Effects of Marine Benthos on Physical Properties of Sediments, Springer, Boston, MA, 3–52, https://doi.org/10.1007/978-1-4757-1317-6_1, 1982.

Rhoads, D. C. and Stanley, D. J.: Biogenic Graded Bedding, SEPM Journal of Sedimentary Research, Vol. 35, 956–963, https://doi.org/10.1306/74d713bb-2b21-11d7-8648000102c1865d, 1965.

Rhodes, E. J.: Optically stimulated luminescence dating of sediments over the past 200,000 years, Annu Rev Earth

935 Planet Sci, 39, 461–488, https://doi.org/10.1146/annurev-earth-040610-133425, 2011.

Richter, R.: Fluidal-Textur in Sediment-Gesteinen und über Sedifluktion überhaupt, Notizbl Hess Landesamtes Bodenforsch Wiesb, 6, 67–81, 1952.

Richter, T. O., Van Der Gaast, S., Koster, B., Vaars, A., Gieles, R., De Stigter, H. C., De Haas, H., and Van Weering, T. C. E.: Modeling 210Pb-derived mixing activity in ocean margin sediments: Diffusive versus nonlocal

940 mixing, J Mar Res, 54, 1207–1227, https://doi.org/10.1357/0022240963213808, 1996.

Richter, T. O., Van Der Gaast, S., Koster, B., Vaars, A., Gieles, R., De Stigter, H. C., De Haas, H., and Van Weering, T. C. E.: The Avaatech XRF Core Scanner: Technical description and applications to NE Atlantic sediments, Geol Soc Spec Publ, 267, 39–50, https://doi.org/10.1144/GSL.SP.2006.267.01.03, 2006.

Riisgård, H. U. and Banta, G. T.: Irrigation and deposit feeding by the lugworm Arenicola marina, characteristics

945 and secondary effects on the environment. A review of current knowledge., Vie et Milieu / Life & Environment, 48, 243–257, 1998.

Ritchie, R. J.: Consistent sets of spectrophotometric chlorophyll equations for acetone, methanol and ethanol solvents, Photosynth Res, 89, 27–41, https://doi.org/10.1007/s11120-006-9065-9, 2006.

Román-Sánchez, A., Reimann, T., Wallinga, J., and Vanwalleghem, T.: Bioturbation and erosion rates along the

950 soil-hillslope conveyor belt, part 1: Insights from single-grain feldspar luminescence, Earth Surf Process Landf, 44, 2051–2065, https://doi.org/10.1002/esp.4628, 2019.

Schneider, C. A., Rasband, W. S., and Eliceiri, K. W.: NIH Image to ImageJ: 25 years of image analysis, https://doi.org/10.1038/nmeth.2089, 28 July 2012.

Self, R. and Jumars, P.: Cross-phyletic patterns of particle selection by deposit feeders, J Mar Res, 46, 1988.

955 Smedley, R. K., Duller, G. A. T., and Roberts, H. M.: Bleaching of the post-IR IRSL signal from individual grains of K-feldspar: Implications for single-grain dating, Radiat Meas, 79, 33–42, https://doi.org/10.1016/j.radmeas.2015.06.003, 2015.

Snelgrove, P. V. R., Soetaert, K., Solan, M., Thrush, S., Wei, C. L., Danovaro, R., Fulweiler, R. W., Kitazato, H., Ingole, B., Norkko, A., Parkes, R. J., and Volkenborn, N.: Global Carbon Cycling on a Heterogeneous Seafloor,

960 Trends Ecol Evol, 33, 96–105, https://doi.org/10.1016/j.tree.2017.11.004, 2018.

Soissons, L. M., Gomes da Conceiçâo, T., Bastiaan, J., van Dalen, J., Ysebaert, T., Herman, P. M. J., Cozzoli, F., and Bouma, T. J.: Sandification vs. muddification of tidal flats by benthic organisms: A flume study, Estuar Coast Shelf Sci, 228, https://doi.org/10.1016/j.ecss.2019.106355, 2019.

Staudt, F., Mullarney, J. C., Pilditch, C. A., and Huhn, K.: Effects of grain-size distribution and shape on sediment
965   bed stability, near-bed flow and bed microstructure, Earth Surf Process Landf, 44, 1100–1116,
https://doi.org/10.1002/esp.4559, 2019.

Stockmann, U., Minasny, B., Pietsch, T. J., and McBratney, A. B.: Quantifying processes of pedogenesis using
optically stimulated luminescence, Eur J Soil Sci, 64, 145–160, https://doi.org/10.1111/ejss.12012, 2013.

van Straaten, L. M. J. U.: Biogene textures and the formation of shell beds in the Dutch Wadden Sea I, Proc.
970   Koninkl. Ned. Akad. Wetenschap, 55, 1952.

Sun, M.-Y., Lee, C., and Aller, R. C.: Laboratory studies of oxic and anoxic degradation of chlorophyll-a in Long
Island Sound sediments, Geochim Cosmochim Acta, 57, 147–157, https://doi.org/10.1016/0016-7037(93)90475-
C, 1993.

Taghon, G. L.: Optimal foraging by deposit-feeding invertebrates: Roles of particle size and organic coating,
975   Oecologia, 52, 295–304, https://doi.org/10.1007/BF00367951, 1982.

Vandenberghe, D., De Corte, F., Buylaert, J. P., Kučera, J., and Van den Haute, P.: On the internal radioactivity
in quartz, Radiat Meas, 43, 771–775, https://doi.org/10.1016/j.radmeas.2008.01.016, 2008.

de Vet, P. L. M., van Prooijen, B. C., Schrijvershof, R. A., van der Werf, J. J., Ysebaert, T., Schrijver, M. C., and
Wang, Z. B.: The Importance of Combined Tidal and Meteorological Forces for the Flow and Sediment Transport
980   on Intertidal Shoals, J Geophys Res Earth Surf, 123, 2464–2480, https://doi.org/10.1029/2018JF004605, 2018.

de Vet, P. L. M., van Prooijen, B. C., Colosimo, I., Steiner, N., Ysebaert, T., Herman, P. M. J., and Wang, Z. B.:
Variations in storm-induced bed level dynamics across intertidal flats, Sci Rep, 10, 1–15,
https://doi.org/10.1038/s41598-020-69444-7, 2020.

Volkenborn, N., Polerecky, L., Hedtkamp, S. I. C., van Beusekom, J. E. E., and de Beer, D.: Bioturbation and
985   bioirrigation extend the open exchange regions in permeable sediments, Limnol Oceanogr, 52, 1898–1909,
https://doi.org/10.4319/lo.2007.52.5.1898, 2007a.

Volkenborn, N., Hedtkamp, S. I. C., van Beusekom, J. E. E., and Reise, K.: Effects of bioturbation and
bioirrigation by lugworms (Arenicola marina) on physical and chemical sediment properties and implications for
intertidal habitat succession, Estuar Coast Shelf Sci, 74, 331–343, https://doi.org/10.1016/j.ecss.2007.05.001,
990   2007b.

Wallinga, J.: On the detection of OSL age overestimation using single-aliquot techniques, Geochronometria:
Journal on Methods & Applications of Absolute Chronology, 21, 17–26, 2002.

Wallinga, J., Hobo, N., Cunningham, A. C., Versendaal, A. J., Makaske, B., and Middelkoop, H.: Sedimentation
rates on embanked floodplains determined through quartz optical dating, Quat Geochronol, 5, 170–175,
995   https://doi.org/10.1016/j.quageo.2009.01.002, 2010.

Wallinga, J., Sevink, J., Van Mourik, J. M., and Reimann, T.: Luminescence dating of soil archives. Reading the
soil archives: unraveling the geoecological code of palaeosols and sediment cores., edited by: van Mourik, J. and
van der Meer, J., Elsevier, Amsterdam, 115–162, https://doi.org/10.1016/B978-0-444-64108-3.00004-5, 2019.

Wang, P. and Cheng, J.: Storm Impacts on the Morphology and Sedimentology of Open-Coast Tidal Flats, in:
1000   Coastal Storms: Processes and Impacts, Wiley Blackwell, 81–98, https://doi.org/10.1002/9781118937099.ch5,
2016.

Ward, J. E. and Shumway, S. E.: Separating the grain from the chaff: Particle selection in suspension- and deposit-
feeding bivalves, J Exp Mar Biol Ecol, 300, 83–130, https://doi.org/10.1016/j.jembe.2004.03.002, 2004.

Wendelboe, K., Egelund, J. T., Flindt, M. R., and Valdemarsen, T.: Impact of lugworms (Arenicola marina) on
1005   mobilization and transport of fine particles and organic matter in marine sediments, J Sea Res, 76, 31–38,
https://doi.org/10.1016/j.seares.2012.10.013, 2013.

Wheatcroft, R. A.: Preservation potential of sedimentary event layers, Geology, 18, 843–845,
https://doi.org/10.1130/0091-7613(1990)018<0843:PPOSEL>2.3.CO;2, 1990.

Widdows, J. and Brinsley, M.: Impact of biotic and abiotic processes on sediment dynamics and the consequences
1010   to the structure and functioning of the intertidal zone, J Sea Res, 48, 143–156, https://doi.org/10.1016/S1385-
1101(02)00148-X, 2002.

Witbaard, R., Bergman, M. J. N., van Weerlee, E., and Duineveld, G. C. A.: An estimation of the effects of Ensis
directus on the transport and burial of silt in the near-shore Dutch coastal zone of the North Sea, J Sea Res, 127,
95–104, https://doi.org/10.1016/j.seares.2016.12.001, 2017.

1015   Zhang, A., Long, H., Yang, F., Zhang, J., Peng, J., and Zhang, G.: Luminescence dating illuminates soil evolution,
Earth Sci Rev, 265, 105103, https://doi.org/10.1016/j.earscirev.2025.105103, 2025.

Zhou, Z., Liu, Q., Fan, D., Coco, G., Gong, Z., Möller, I., Xu, F., Townend, I., and Zhang, C.: Simulating the role
of tides and sediment characteristics on tidal flat sorting and bedding dynamics, Earth Surf Process Landf, 46,
2163–2176, https://doi.org/10.1002/esp.5166, 2021.

1020   Zhou, Z., Wu, Y., Fan, D., Wu, G., Luo, F., Yao, P., Gong, Z., and Coco, G.: Sediment sorting and bedding
dynamics of tidal flat wetlands: Modeling the signature of storms, J Hydrol (Amst), 610, 127913,
https://doi.org/10.1016/j.jhydrol.2022.127913, 2022.

Ziegler, M., Jilbert, T., de Lange, G. J., Lourens, L. J., and Reichart, G.: Bromine counts from XRF scanning as
an estimate of the marine organic carbon content of sediment cores, Geochemistry, Geophysics, Geosystems, 9,
1025   https://doi.org/10.1029/2007GC001932, 2008.